Laboratory Validation of an Endurance Limit for Asphalt Pavements

AUTHORS

Witczak, Matthew; Mamlouk, Michael; Souliman, Mena; Zeiada, Waleed

BUY THIS BOOK

FIND RELATED TITLES

Visit the National Academies Press at **NAP.edu** and login or register to get:

– Access to free PDF downloads of thousands of scientific reports
– 10% off the price of print titles
– Email or social media notifications of new titles related to your interests
– Special offers and discounts

NATIONAL COOPERATIVE HIGHWAY RESEARCH PROGRAM

NCHRP REPORT 762

Laboratory Validation of an Endurance Limit for Asphalt Pavements

Matthew Witczak
Michael Mamlouk
ARIZONA STATE UNIVERSITY
Tempe, Arizona

Mena Souliman
UNIVERSITY OF NEVADA
Reno, Nevada

Waleed Zeiada
ARIZONA STATE UNIVERSITY
Tempe, Arizona

Subscriber Categories
Highways • Design • Materials

TRANSPORTATION RESEARCH BOARD

WASHINGTON, D.C.
2013
www.TRB.org

NATIONAL COOPERATIVE HIGHWAY RESEARCH PROGRAM

Systematic, well-designed research provides the most effective approach to the solution of many problems facing highway administrators and engineers. Often, highway problems are of local interest and can best be studied by highway departments individually or in cooperation with their state universities and others. However, the accelerating growth of highway transportation develops increasingly complex problems of wide interest to highway authorities. These problems are best studied through a coordinated program of cooperative research.

In recognition of these needs, the highway administrators of the American Association of State Highway and Transportation Officials initiated in 1962 an objective national highway research program employing modern scientific techniques. This program is supported on a continuing basis by funds from participating member states of the Association and it receives the full cooperation and support of the Federal Highway Administration, United States Department of Transportation.

The Transportation Research Board of the National Academies was requested by the Association to administer the research program because of the Board's recognized objectivity and understanding of modern research practices. The Board is uniquely suited for this purpose as it maintains an extensive committee structure from which authorities on any highway transportation subject may be drawn; it possesses avenues of communications and cooperation with federal, state and local governmental agencies, universities, and industry; its relationship to the National Research Council is an insurance of objectivity; it maintains a full-time research correlation staff of specialists in highway transportation matters to bring the findings of research directly to those who are in a position to use them.

The program is developed on the basis of research needs identified by chief administrators of the highway and transportation departments and by committees of AASHTO. Each year, specific areas of research needs to be included in the program are proposed to the National Research Council and the Board by the American Association of State Highway and Transportation Officials. Research projects to fulfill these needs are defined by the Board, and qualified research agencies are selected from those that have submitted proposals. Administration and surveillance of research contracts are the responsibilities of the National Research Council and the Transportation Research Board.

The needs for highway research are many, and the National Cooperative Highway Research Program can make significant contributions to the solution of highway transportation problems of mutual concern to many responsible groups. The program, however, is intended to complement rather than to substitute for or duplicate other highway research programs.

NOTICE

The project that is the subject of this report was a part of the National Cooperative Highway Research Program, conducted by the Transportation Research Board with the approval of the Governing Board of the National Research Council.

The members of the technical panel selected to monitor this project and to review this report were chosen for their special competencies and with regard for appropriate balance. The report was reviewed by the technical panel and accepted for publication according to procedures established and overseen by the Transportation Research Board and approved by the Governing Board of the National Research Council.

The opinions and conclusions expressed or implied in this report are those of the researchers who performed the research and are not necessarily those of the Transportation Research Board, the National Research Council, or the program sponsors.

The Transportation Research Board of the National Academies, the National Research Council, and the sponsors of the National Cooperative Highway Research Program do not endorse products or manufacturers. Trade or manufacturers' names appear herein solely because they are considered essential to the object of the report.

THE NATIONAL ACADEMIES
Advisers to the Nation on Science, Engineering, and Medicine

The **National Academy of Sciences** is a private, nonprofit, self-perpetuating society of distinguished scholars engaged in scientific and engineering research, dedicated to the furtherance of science and technology and to their use for the general welfare. On the authority of the charter granted to it by the Congress in 1863, the Academy has a mandate that requires it to advise the federal government on scientific and technical matters. Dr. Ralph J. Cicerone is president of the National Academy of Sciences.

The **National Academy of Engineering** was established in 1964, under the charter of the National Academy of Sciences, as a parallel organization of outstanding engineers. It is autonomous in its administration and in the selection of its members, sharing with the National Academy of Sciences the responsibility for advising the federal government. The National Academy of Engineering also sponsors engineering programs aimed at meeting national needs, encourages education and research, and recognizes the superior achievements of engineers. Dr. C. D. Mote, Jr., is president of the National Academy of Engineering.

The **Institute of Medicine** was established in 1970 by the National Academy of Sciences to secure the services of eminent members of appropriate professions in the examination of policy matters pertaining to the health of the public. The Institute acts under the responsibility given to the National Academy of Sciences by its congressional charter to be an adviser to the federal government and, on its own initiative, to identify issues of medical care, research, and education. Dr. Harvey V. Fineberg is president of the Institute of Medicine.

The **National Research Council** was organized by the National Academy of Sciences in 1916 to associate the broad community of science and technology with the Academy's purposes of furthering knowledge and advising the federal government. Functioning in accordance with general policies determined by the Academy, the Council has become the principal operating agency of both the National Academy of Sciences and the National Academy of Engineering in providing services to the government, the public, and the scientific and engineering communities. The Council is administered jointly by both Academies and the Institute of Medicine. Dr. Ralph J. Cicerone and Dr. C. D. Mote, Jr., are chair and vice chair, respectively, of the National Research Council.

The **Transportation Research Board** is one of six major divisions of the National Research Council. The mission of the Transportation Research Board is to provide leadership in transportation innovation and progress through research and information exchange, conducted within a setting that is objective, interdisciplinary, and multimodal. The Board's varied activities annually engage about 7,000 engineers, scientists, and other transportation researchers and practitioners from the public and private sectors and academia, all of whom contribute their expertise in the public interest. The program is supported by state transportation departments, federal agencies including the component administrations of the U.S. Department of Transportation, and other organizations and individuals interested in the development of transportation. **www.TRB.org**

www.national-academies.org

COOPERATIVE RESEARCH PROGRAMS

FOREWORD

By Edward Harrigan
Staff Officer
Transportation Research Board

This report presents models for the HMA fatigue endurance limit that are responsive to asphalt binder and mixture properties and healing between load cycles and are suitable for incorporation as algorithms in Pavement ME Design and other design methods. Thus, the report will be of immediate interest to materials and structural design engineers in state highway agencies and engineers in the HMA construction industry.

Many well-constructed flexible pavements with a thick HMA structure have been in service for 40 or more years without any evidence of fatigue cracking. This field experience suggests that an endurance limit, that is, a level of strain below which fatigue damage does not accumulate for any number of load repetitions, is a valid concept for HMA mixtures.

NCHRP Project 9-38, "Endurance Limit of Hot Mix Asphalt Mixtures to Prevent Fatigue Cracking in Flexible Pavements," completed in 2009, confirmed the existence of an HMA fatigue endurance limit through an extensive program of laboratory testing, which further suggested that the endurance limit is influenced by HMA mixture and binder properties. Based on these results, a practical definition of the endurance limit was developed, along with a method to estimate its value in the laboratory.

NCHRP Project 9-44A was designed to extend the results and findings of Project 9-38, with particular attention to the influence of asphalt binder and mixture properties on the endurance limit and to the relationship of the endurance limit to the phenomenon of healing hypothesized to occur in asphalt mixtures during the rest period between load applications in the laboratory and in pavements. The specific objectives of the project were to (1) carry out a laboratory experiment to identify the mixture and pavement layer design features related to an endurance limit for bottom-initiated fatigue cracking of HMA and (2) develop an algorithm to incorporate this endurance limit into the Pavement ME Design software and other selected pavement design methods. The research was performed by Arizona State University, Tempe, Arizona, in association with AMEC (formerly MACTEC), Phoenix, Arizona.

The research investigated the relationship of the fatigue endurance limit to factors such as asphalt binder rheology, air voids, asphalt content, temperature, strain level, number of load cycles, and rest period between load cycles. Both beam fatigue (AASHTO T321) and uniaxial compression-tension testing were conducted according to a factorial design that permitted statistical analysis of the main factor and up to three-factor interactions. Robust regression models were developed that described the effect of the main factors and factor interactions on the stiffness ratio, SR, which is defined as the ratio of the stiffness measured at any load cycle during beam fatigue or uniaxial fatigue testing to the initial stiffness of the specimen. Testing was conducted with rest periods of 0, 1, 5, and 10s between load cycles.

The endurance limit can then be determined for any mixture initial stiffness as the strain at SR = 1, i.e., for the condition in which complete healing of the fatigue damage takes place after each load cycle.

Thus, this research reaffirmed the existence of the HMA fatigue endurance limit and demonstrated that the endurance limit is the result of a balance between loading damage and the healing, i.e., damage recovery, that happens during rest periods and that the value of the limit varies with the mixture initial stiffness (acting as a surrogate for binder rheology, air voids, asphalt content, and temperature) and the duration of the rest period. It was also found that for a load cycle of 0.1s, a rest period greater than 5 to 10s (from beam fatigue testing) or greater than 3s (from uniaxial testing) will not produce additional healing of the fatigue damage in the laboratory. Finally, the report recommends that the beam fatigue model be used for future study of the endurance limit and its implementation. The beam fatigue test is better established than the uniaxial test and has a larger database of results in the literature.

This report fully documents the research and discusses incorporation of the endurance limit derived from the SR regression model formalism as an algorithm in Pavement ME Design software and other design methods. The report includes three appendixes available online at http://apps.trb.org/cmsfeed/TRBNetProjectDisplay.asp?ProjectID=2518:

- Appendix 1, Integrated Predictive Model for Healing and Fatigue Endurance Limit for Asphalt Concrete
- Appendix 2, Endurance Limit for HMA Based on Healing Phenomena Using Viscoelastic Continuum Damage Analysis
- Appendix 3, Project Lab Test Results Inserted into the Mechanistic Empirical Distress Prediction Models (M-E_DPM) Database

C O N T E N T S

Note: Many of the photographs, figures, and tables in this report have been converted from color to grayscale for printing. The electronic version of the report (posted on the Web at www.trb.org) retains the color versions.

CHAPTER 1

Introduction

Bottom-up fatigue cracking is one of the main distress types in flexible pavement. Current design methods of flexible pavement assume that cumulative damage occurs where each load cycle uses up a portion of the finite fatigue life of the asphalt layer regardless of load magnitude or traffic volume. The concept of endurance limit assumes that there is a strain value below which fatigue damage may not occur or can be healed during unloading. The fact that traffic loads are separated by "rest periods" may allow for partial or full healing of the accumulated damage, which in turn increases the number of load repetitions before failure. Therefore, if the pavement is thick enough to keep strains below the endurance limit, the fatigue life of the pavement can be considerably extended. This concept has significant design and economic implications.

In 1972, Monismith and McLean (1) first proposed an endurance limit of 70 microstrain for asphalt pavements. More recently, Nishizawa et al. (2) analyzed in-service pavements in Japan and reported an endurance limit of 200 microstrain. Wu et al. back-calculated Falling Weight Deflectometer (FWD) data and reported strains at the bottom of the asphalt layer between 96 and 158 microstrain for a long-life pavement in Kansas (3). Bhattacharjee et al. (4) obtained endurance limit values through uniaxial testing that ranged from 115 to 250 microstrain. Studies performed at the University of Illinois (5, 6) showed that fatigue life becomes significantly longer if the strain is kept below approximately 100 microstrain. In NCHRP Project 9-38, beam fatigue and uniaxial tension testing were conducted to determine fatigue life (7). By conducting a small strain-controlled beam fatigue test, a fatigue life in excess of 50 million cycles was achieved. Data from the Long Term Pavement Performance (LTPP) studies were also analyzed to determine if they support the endurance limit concept. The results obtained from the study support the existence of an endurance limit in HMA mixes (7).

Another major concept recently investigated by researchers is the HMA healing phenomenon. Healing of micro-damage was proposed as the primary reason for the increased fatigue life at low strain levels (8, 9, 10). Healing is generally considered as the capability of a material to self-recover its mechanical properties (stiffness or strength) to some extent upon resting due to the closure of micro-cracks. Phillips (11) proposed that healing of asphalt binders is a three-step process consisting of (1) the closure of micro-cracks due to wetting (adhesion of two crack surfaces together driven by surface energy); (2) the closure of macro-cracks due to consolidating stresses and binder flow; and (3) the complete recovery of mechanical properties due to diffusion of asphaltene structures. Kim and Little (12) developed a mechanical approach to identify the healing potential of asphalt concrete. They performed cyclic loading tests with varying rest periods on notched beam specimens of sand asphalt mixtures. They concluded that rest periods enhance the fatigue life through healing and relaxation mechanisms.

There is mounting evidence that healing and the endurance limit of HMA are related to each other. It has been observed both in laboratory studies of fatigue at low strain levels with rest periods and in thick, properly constructed pavements that bottom-initiated fatigue cracking is almost non-existent. The HMA endurance limit, however, does not reflect an absence of load induced damage in the HMA. Rather, it results from a balance of damage caused by loading and healing or damage recovery occurring during rest periods (6). The endurance limit of HMA is, therefore, not a single value, but varies depending on loading and environmental conditions applied to the HMA. Considering an endurance limit in flexible pavement design requires the consideration of the effects of loading, environment, and material properties on both damage accumulation and healing. These findings on the endurance limit of HMA served as the research hypothesis upon which NCHRP Project 9-44 (13) was formulated.

In summary, the literature provides endurance limit values for certain conditions, but there is no general predictive model currently available to estimate these values under

different conditions and accounting for healing. Also, the literature does not provide a clear relationship between endurance limit and healing, which is one of the main contributions of this research.

Previous studies showed that fatigue life is primarily influenced by mix stiffness (E) and also affected by binder content and air voids. Lower asphalt contents and lower air voids led to higher stiffness, while higher asphalt contents and lower air voids led to higher fatigue lives (14, 15). Tayebali et al. (16) also found that as air voids increased, fatigue life decreased for both controlled strain and controlled stress tests. It was concluded that stiffer mixes would perform better for thick pavements, while lower stiffness mixes would perform better for thin pavements.

Fatigue life and endurance limit are also affected by temperature and binder grade. Because the endurance limit of HMA is tied closely to the healing potential of the binder, healing occurs more rapidly at higher temperatures and softer binder grades, and the strain level that can be tolerated with no damage accumulation is increased (9). Verstraeten et al. (17) concluded that the longer the rest periods and the higher the temperatures, the greater the beneficial effect.

Over the last 50 years, several researchers have studied the significance of rest periods between load applications during fatigue testing of HMA. Different findings have been presented in the literature showing different opinions on the effect of rest period. Some researchers thought that the rest period only leads to a temporary modulus recovery without actually extending the fatigue life, while others found that the modulus recovery did extend fatigue life by a certain amount.

Van Dijk and Visser (18) found that increased rest periods can increase fatigue life by a factor of 1 to 10 times. Other test results indicated that increasing the rest period had no significant effect on fatigue performance under certain assumptions and test conditions (19). Raithby and Sterling (20) found that fatigue life does not increase significantly for rest periods greater than ten times the loading time (or 1s rest period) and the waveform influence was less important than the duration of rest periods. Van Dijk and Visser (18) showed increased fatigue lives with increasing rest periods. Bonnaure et al. (21) concluded that increasing the rest period between the loading cycles increases fatigue life. They also showed that the maximum beneficial effect of rest periods on the fatigue life was for a rest period equal to 25 times the loading cycle (or 0.625s).

Objectives

The objectives of this research were to (1) determine the fatigue endurance limit for HMA and relate it to healing that occurs during the rest period between load applications and (2) develop models that relate the endurance limit of HMA to material properties, loading conditions, and temperature.

These objectives were achieved by conducting both beam and uniaxial fatigue laboratory experiments to identify the mixture and pavement design features related to the endurance limit for bottom-initiated fatigue cracking. Issues studied included incorporating rest periods between loading cycles and the effect of rest period on the healing and endurance limit of HMA.

This report summarizes the design, features, results, and products of the beam fatigue and uniaxial fatigue experiments conducted in NCHRP Project 9-44A to meet these objectives.

Appendixes 1 and 2 are comprehensive treatises describing all aspects of the beam fatigue and uniaxial fatigue studies, respectively, including tabulations of the experimental data. These appendixes are adapted from dissertations presented by Dr. Mena Souliman and Dr. Waleed Zeiada to Arizona State University in partial fulfillment of the requirements for their Doctor of Philosophy degrees. Appendix 3 is a description of the Microsoft Access® Mechanistic-Empirical Distress Prediction Models (M-E_DPM) database in which all relevant data and results from the project are stored.

Appendixes 1, 2, and 3, and the M-E_DPM database are not published herein, but are available online on the TRB website (http://trb.org) and can be found by searching for *NCHRP Report 762*.

HMA Endurance Limit and Healing

A rational procedure was developed to relate the HMA healing phenomenon to the endurance limit. If the fatigue test is conducted with and without rest period between load applications, the typical stiffness ratio (SR) (ratio between the current stiffness and the initial stiffness) versus the number of load cycles will be as shown in Figure 1. Both curves start at an SR of one (no damage). The curve for the test without rest period is steeper than the other curve because of the continuous deterioration during the test. The test with rest period shows higher SR values during the test because of healing that
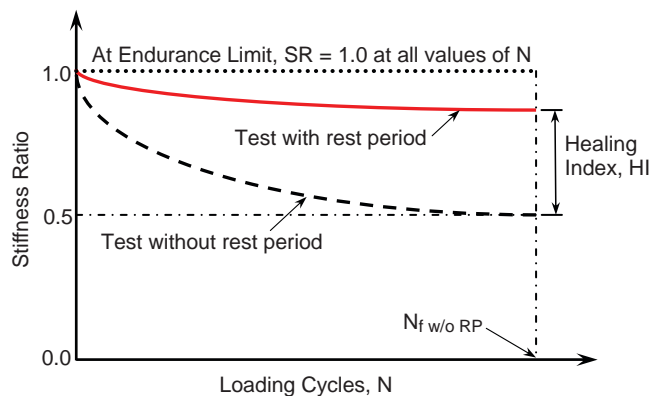

Figure 1. Typical SR versus number of load cycles for tests with and without rest period.

occurs during the rest period after each load application. A larger separation between the two curves indicates more healing, and vice versa. If the curve for the test with rest period remains horizontal, it indicates that full healing occurs after each load cycle.

Healing Index (HI) (Equation 1) was defined as the difference between the SRs for the tests with and without rest period at $N_{f\,w/o\,RP}$ (number of cycles to failure for the test without rest period) as shown in Figure 1, where failure is defined when the SR reaches 0.5.

$$HI = \left[SR_{w/RP} - SR_{w/o\,RP}\right]_{at} N_{f\,w/o\,RP} \qquad (1)$$

where,

    $SR_{w/RP}$ = stiffness ratio with rest period
    $SR_{w/o\,RP}$ = stiffness ratio without rest period

The approach used in this research is to develop a regression relation between SR and various factors in the form of Equation 2:

$$SR = f\left(BG, AC, V_a, T, \varepsilon, N, RP\right) \qquad (2)$$

In Equation 2, SR is the stiffness ratio, BG is the binder grade, AC is the binder content, V_a is the air voids, T is the temperature, ε is the initial strain, N is the number of load applications, and RP is the rest period between load applications.

If the SR in Equation 2 is set to one, the strain, ε, will become the endurance limit, which implies that full healing occurs after each loading cycle. Note that an SR of 1 is equivalent to an HI of 0.5, which means full healing. Note also that setting the SR to 1 to determine the endurance limit is a better approach than setting the HI to 0.5. The SR approach can be used at any number of load repetitions (N), but the HI approach can be used at $N_{f\,w/o\,RP}$ only. Also, since it is assumed that full healing occurs after each loading cycle at the endurance limit, the number of loading cycles is redundant and may be removed from Equation 2 without large effect.

The rest period in the laboratory is inversely related to the average annual daily truck traffic (AADTT) in the field. If the AADTT is low, the time between trucks or axle loads is large, which corresponds to large rest periods between stress applications.

Materials, Mix Design, and Fatigue Testing

A 19-mm Superpave mix design was selected for the project that met the requirements of typical mixtures used for paving arterial roads in Arizona (22). Three asphalt concrete mixes using three binder grades (PG 58-28, PG 64-22, and
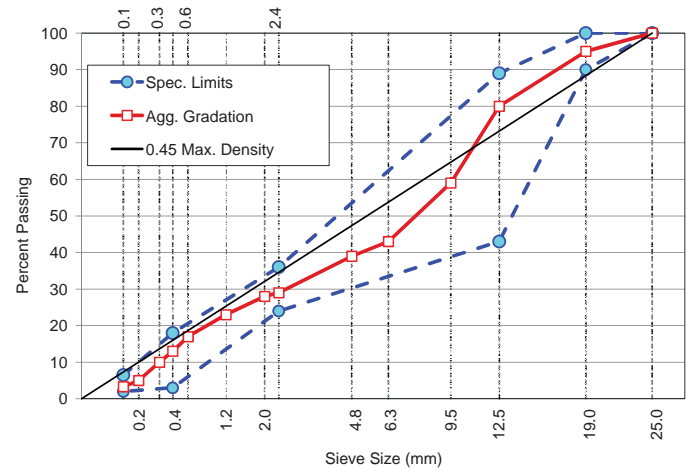
Figure 2. Designed aggregate gradation distribution.

PG 76-16) were prepared to ensure that a wide range of stiffness would be encountered. The same aggregate gradation was used for all three mixtures. Figure 2 shows the designed aggregate gradation distribution curve and the specification limits and Table 1 shows the composite aggregate properties.

Mixes were designed according to the requirements of Maricopa Association of Governments (MAG) 710 specifications (22) for High Traffic Gyratory mixes with $N_{design} = 100$. Table 2 shows the volumetric mix design for the three binders. The optimum binder contents were 4.8, 4.5, and 4.7 percents for the PG 58-28, PG 64-22, and PG 76-16 mixtures, respectively.

Two types of fatigue tests were conducted, beam (flexure) fatigue and uniaxial fatigue. Beam fatigue tests were performed on HMA mixtures prepared with all three binder grades (PG 58-28, PG 64-22, and PG 76-16), whereas the uniaxial fatigue tests were performed on asphalt mixtures prepared with the PG 64-22 binder grade only.

Table 1. Composite aggregate properties.

Property	Value	Specifications
Bulk (Dry) Sp. Gravity	2.614	2.35-2.85
SSD Sp. Gravity	2.638	—
Apparent Sp. Gravity	2.677	—
Water Absorption (%)	0.90	0-2.5
Sand Equivalent Value	71	Min 50
Fractured Face One (%)	99	Min 85
Fractured Face Two (%)	96	Min 80
Flat & Elongation (%)	1.0	Max 10
Uncompacted Voids (%)	46.8	Min 45
L.A. Abrasion @ 500 Rev.	16	Max 40

Table 2. Volumetric mix design for different binder types.

Volumetric Property	Binder Type			Specifications
	PG 58-28	PG 64-22	PG 76-16	
Target Asphalt Content (%)	4.8	4.5	4.7	4.5-5.5
Bulk Specific Gravity (G_{mb})	2.365	2.367	2.351	N/A
Theoretical Max. Sp. Gr. (G_{mm})	2.461	2.467	2.454	N/A
Design Air Voids (%)	3.9	4.1	4.2	3.8-4.2
VMA (%)	13.9	13.5	14.3	Min. 13
VFA (%)	71.9	69.9	70.8	N/A
Asphalt Sp. Gr. (G_b)	1.024	1.024	1.042	N/A

Developing of Endurance Limit Model Based on Beam Fatigue Tests

Beam Fatigue Testing

Beams were prepared using vibratory loading applied by a servohydraulic loading machine. A mold was used with inside dimensions larger than the required dimensions of the beam to allow for sawing to achieve standardized specimen dimensions. The mix was compacted using a stress-controlled sinusoidal load to reach a pre-determined density. The beams were brought to the required dimensions of $15 \times 2 \times 2.5$ in. for fatigue testing by sawing ¼ in. from each side. Air voids were measured using the saturated surface-dry procedure (AASHTO T166, Method A). Any specimen with air voids deviating by more than 1 percent from the target value of 7 percent was rejected. The details of beam preparation and verification of air void uniformity within the specimen are presented elsewhere (23). Fatigue tests were performed using the beam fatigue test apparatus shown in Figure 3.

Sinusoidal versus Haversine Waveforms

Before testing, a pilot study (24) was performed using the PG 64-22 mixture to compare haversine and sinusoidal waveforms (see Figure 4), especially when incorporating rest periods between load cycles that cause healing of the HMA. Deflection-controlled haversine and sinusoidal flexure beam fatigue test protocols are defined in ASTM D7460 and AASHTO T321, respectively.

Figure 5 illustrates what happens (hypothetically) to an HMA beam during the sinusoidal deflection-controlled test and the haversine deflection-controlled test. In the sinusoidal test (Figure 5[a]), the deflection input is sinusoidal, which bends the beam in both directions. The neutral position of the beam does not change during the test and remains in the original position halfway between the two extreme positions. In the haversine test (Figure 5[b]), the deflection input is haversine, which bends the beam with the same peak-to-peak magnitude as the sinusoidal test but in one direction only. Because of the viscous response of the material, creep (permanent deformation) occurs in the beam and the neutral position of the beam shifts downward after a few loading cycles. The neutral position is located halfway between the extreme positions and the haversine deflection transitions to a sinusoidal deflection performed on a bent beam.

Figure 6 illustrates the deflection input and the stress and strain outputs that occur in the HMA beam during the test. Since the neutral position of the beam does not change in the sinusoidal test, the developed strain and stress are sinusoidal, causing alternating tension and compression in the beam as shown in Figure 6 (a). In the haversine test, the deflection input remains haversine throughout the test. The developed strain and stress pulses start as haversine waveforms causing strain and stress in one direction (compression at the top of the beam and tension at the bottom without reversal). Because of the shifted position of the beam, however, the developed strain and stress pulses immediately change to sinusoidal causing alternating tension and compression with one-half of the magnitude of the stress applied at the beginning of the test as shown in Figure 6 (b). At the end of the test, when the load is removed, the beam remains in the bent position showing permanent deformation. The permanent deformation at the center of the beam at the end of the test is equal to one-half of the peak-to-peak deflection during the test. For example, if a 400 peak-to-peak microstrain is maintained during the test, a peak-to-peak deflection of 0.009 in. is produced and 0.0045 in. of permanent deformation would result at the end of the test. Although this permanent deformation is not seen with the naked eye, it produces erroneous fatigue and endurance limit results since the calculations do not match the test conditions. This pilot study observation confirmed the conclusions of Pronk (25, 26).

Therefore, it was concluded that the deflection-controlled sinusoidal test (AASHTO T321) is more consistent than the deflection-controlled haversine test (ASTM D7460) since it produces the intended stress and strain waveform. This is particularly important for studies dealing with healing and the endurance limit of HMA, in order to obtain a fair comparison

Figure 4. Haversine and sinusoidal waveforms.

Figure 3. Beam fatigue test apparatus.

of tests with and without rest periods and an accurate assessment of the fatigue and healing results. It was also concluded that in the beam fatigue test on HMA, the loading machine controls the deflection, not the strain. Because of the permanent deformation that occurs in the material, the strain does not match the deflection. Therefore, the so-called haversine "strain-controlled" test on HMA is technically a haversine "deflection-controlled" test.

Based on the results of the pilot study, beam fatigue tests were conducted according to AASHTO T321 test procedure using sinusoidal loading. Some tests were performed without rest periods with a frequency of 10 Hz according to AASHTO T321, while others used a 0.1s sinusoidal loading followed by a rest period. Figure 7 shows the waveform used in the study, which required a software modification in the operating system of the loading machine.

Tests without rest periods were performed up to failure, which occurs when the SR reaches 0.5. Since the tests with rest periods take considerably longer than tests without rest periods, it was decided to run all tests with rest period up to 20,000 cycles only. Extrapolation was then used to predict the SR for the test with rest period at $N_{f \, w/o \, RP}$. Figure 8 shows the extrapolation used to determine the SR for tests with rest period at $N_{f \, w/o \, RP}$.

The accuracy of the extrapolation was verified by running several tests with a rest period until 200,000 cycles. Data points from the first 20,000 cycles were used to extrapolate up to 200,000 and were compared with actual data. It was found that an exponential function was able to extrapolate the data accurately and this process almost exactly predicted the measured data obtained at 200,000 cycles.

Experimental Design

The following factors and levels were used during testing for the beam fatigue endurance limit study.

Figure 5. Neutral and extreme positions using sinusoidal and haversine waveform deflection-controlled test on HMA.

(a) Sinusoidal (AASHTO T321)

(b) Haversine (ASTM D7460)

Figure 6. Stresses, strains, and deflections versus time for sinusoidal and haversine deflection-controlled tests.

Figure 7. Deflection-controlled sinusoidal waveform with rest period used in the study.

Figure 8. Typical extrapolation to estimate stiffness ratio (SR) (with rest period) at $N_{f\,w/o\,RP}$ (PG 64-22, 40F, 4.2% AC, 4.5% V_a, 200 microstrain).

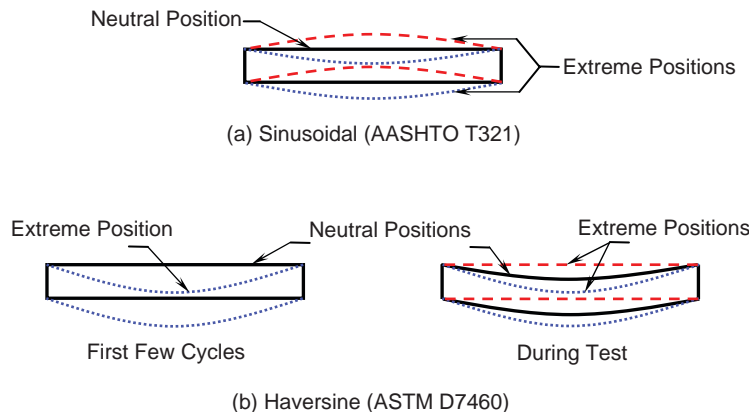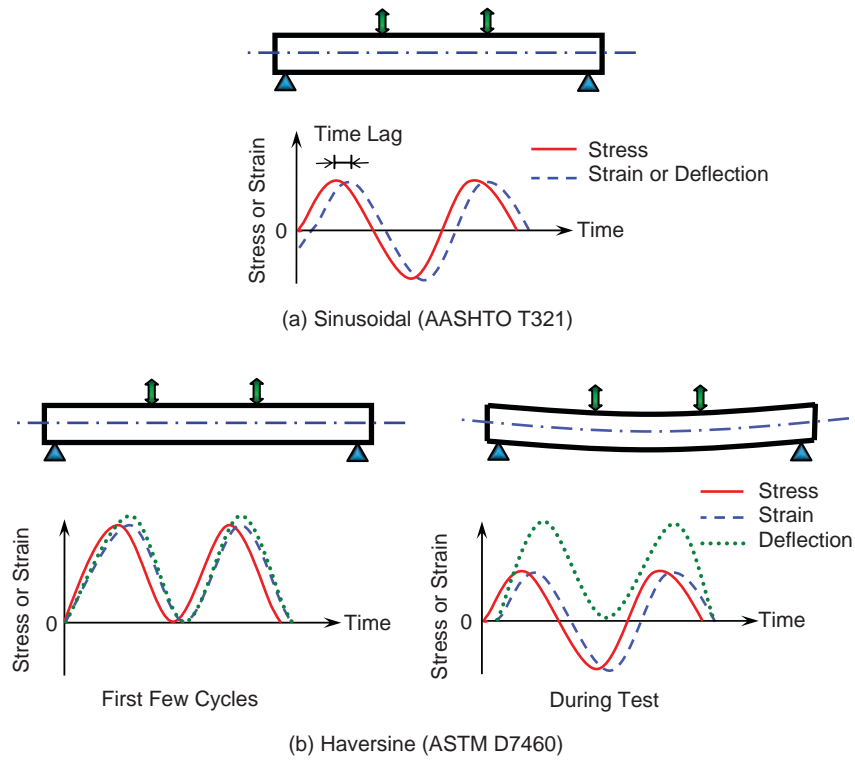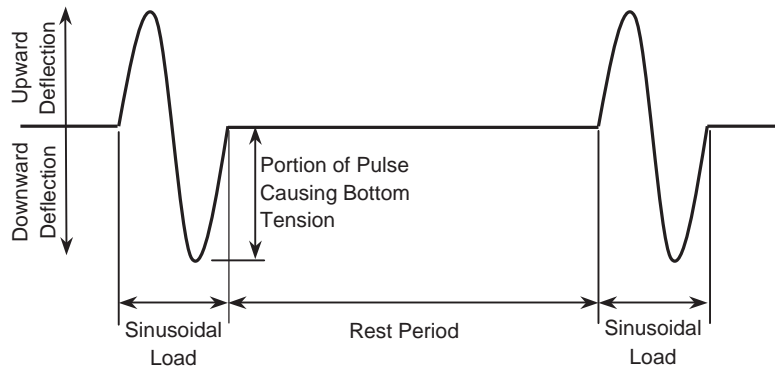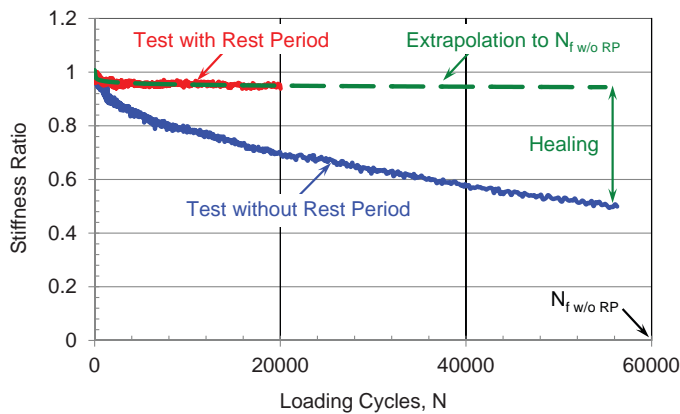1. Binder grade (3 levels: PG 58-28, PG 64-22, PG 76-16)
2. Binder content (2 levels: optimum ± 0.5%)
3. Air voids (2 levels: 4.5, 9.5%)
4. Strain level (3 levels: L, M, H)
5. Temperature (3 levels: 40, 70, 100°F)
6. Rest period (4 levels: 0, 1, 5, 10s)

The criterion for selecting the strain level at each temperature was to reach a fatigue life of approximately 20,000 cycles at the high strain level and approximately 100,000 cycles at the low strain level for tests without rest period ($N_{f\,w/o\,RP}$). These strain levels were determined from pilot beam fatigue tests conducted at different strain levels at 40, 70, and 100°F.

It was clear that a complete factorial design using the previously mentioned factors and levels would be practically impossible considering the time and resources available. Added to the problem is the time it takes to run beam fatigue tests with rest periods. For example, a fatigue test with a 0.1s loading cycle, 5s rest period, and 20,000 load applications takes 28.3 hours, in addition to the time needed for mix preparation, specimen compaction and sawing, and air void determination. Therefore, it was decided to use a six-factor fractional factorial statistical design with partial randomization that would provide accurate results and require fewer tests (*27*). This design allows for determining the effects of the main factors and up to three-factor interactions.

Table 3 shows the factor combinations used in the beam and uniaxial fatigue tests. Three replicates were tested at each factor combination in the first part of the study. An analysis using the PG 64-22 data points was then performed to determine the minimum number of replicates to maintain the required accuracy. The statistical results concluded that the accuracy of the results does not change when using two or three replicates for each factor combination. Therefore, it was decided to use two replicates in the rest of the study. In the beam fatigue study, the results from a total of 468 tests were analyzed to develop the SR model as discussed in the subsequent section.

Model Development

Several trials were made to determine the best mathematical form to relate the independent variables to SR. It was found that there was a need for logarithmic transformations for some variables. It was also concluded that the best mathematical form to relate SR to rest period was the tangent hyperbolic (Tanh) function since it was noted during the laboratory tests that there was no large gain in healing from applying a 10s rest period compared to a 5s rest period. This observation agrees with the literature that showed that there is a threshold rest period beyond which no additional healing is gained.

In an effort to develop a satisfactory relationship between the SR and the material and testing conditions, several regression models were attempted. Originally, a regression model was developed to relate the SR to all factors used in the study, which are binder content, air voids, binder grade, temperature, applied tensile strain, rest period, and number of loading cycles. Later, the model was simplified using the initial stiffness of the mixture as a surrogate for the binder content, air voids, binder grade, and temperature, as all these parameters affect stiffness. This rather innovative approach relates the endurance limit to a basic material property, stiffness. Two main advantages were achieved with this modification. First, the model is simplified. Second, the model is more compatible with the AASHTOWare Pavement ME Design software, where the prediction of pavement performance is mainly driven by the stiffness (or dynamic modulus) of HMA. However, care has to be taken when replacing volumetric properties with the material stiffness since air voids and binder content can counteract each other and create the same stiffness but different endurance limits. This problem was minimized in the development of the beam fatigue model in this study by considering the effect of a wide range of stiffness (three binder grades), which reduced the impact of the stiffness effect.

The model was further refined by adding more data points. As discussed earlier, the applied strain was pre-selected to reach failure for the test without rest period at a certain number of cycles ($N_{f\,w/o\,RP}$). This situation resulted in co-linearity between the strain and the number of cycles. To remove the co-linearity in the model, SR data were collected at three different locations along the SR-N relationship for tests with rest period. Two of these points were taken during the test, while the third point was taken at $N_{f\,w/o\,RP}$. Figure 9 shows the typical SR-N relationships for the tests with and without rest period and the locations where data points were taken. Note that the test results with rest period are extrapolated to $N_{f\,w/o\,RP}$ as discussed earlier.

Table 3. Factor combinations used for the beam and uniaxial fatigue tests.

Legend: ▓ = Beam Fatigue Test (yellow); X = Uniaxial Fatigue Test

Binder Grade →			PG 76-16				PG 64-22				PG 58-28			
Binder Content (%) →			4.2		5.2		4.2		5.2		4.2		5.2	
Air Voids (%) →			4.5	9.5	4.5	9.5	4.5	9.5	4.5	9.5	4.5	9.5	4.5	9.5
Temperature (F)	Strain Level	Rest Period (seconds)												
40°	Low	0	▓	▓	▓	▓	X	X		X	▓	▓	▓	▓
		1				▓						▓		
		5	▓			▓	X	X	X	X		▓	▓	▓
		10												
	Medium	0	▓	▓	▓	▓	X		X	X	▓	▓	▓	▓
		1						X						
		5	▓	▓	▓	▓		X	X	X	▓	▓	▓	▓
		10						X			▓			
	High	0	▓		▓	▓		▓		X	▓			▓
		1						▓	X		▓			▓
		5				▓	X							
		10	▓					▓				▓		
70°	Low	0	▓	▓	▓	▓	X	X	X	▓	▓	▓	▓	▓
		1		▓									▓	
		5	▓		▓	▓	X	X		X	▓	▓	▓	▓
		10						X						
	Medium	0	▓	▓	▓	▓	X	X	▓	X	▓	▓	▓	▓
		1	▓					X						
		5		▓	▓	▓	X	X	X	X	▓	▓	▓	
		10		▓										
	High	0		▓		▓		▓	▓		▓		▓	
		1								X				
		5						▓					▓	
		10				▓					▓			
100°	Low	0	▓	▓	▓	▓	X		X	X	▓	▓	▓	▓
		1					X			X				
		5	▓	▓	▓	▓		X	X		▓		▓	▓
		10									▓			
	Medium	0	▓	▓	▓	▓		X	X	X	▓	▓	▓	▓
		1		▓									▓	
		5	▓		▓		X	X		X	▓			▓
		10			▓			X						▓
	High	0			▓		▓	X		▓	▓	▓	▓	
		1			▓									
		5					▓			X		▓		
		10						▓					▓	

▓ Beam Fatigue Test

X Uniaxial Fatigue Test

Figure 9. Selection of data point locations.

Figure 10. Predicted versus measured SR for the beam fatigue SR model.
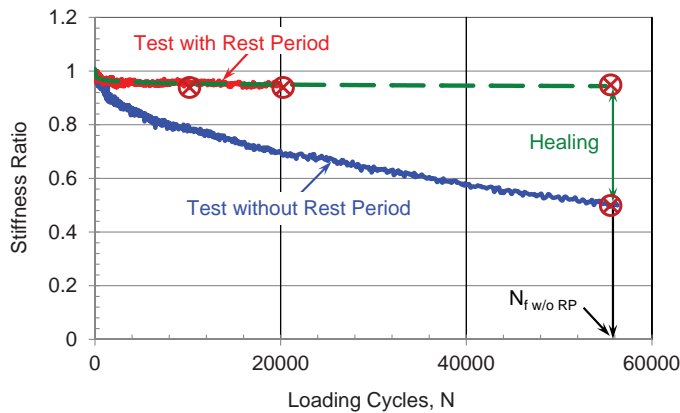
A total of 946 data points was used to build the regression model. Two main statistical software programs were utilized to build the regression model: STATISTICA and Microsoft Excel®. STATISTICA was used to determine the best initial values for the coefficients. An optimization process was then performed using Excel® to minimize the sum of squared error followed by setting the sum of errors equal to zero. The JMP® software (27) was used in developing the model by trying different combinations of factors. A statistical procedure (28) was then used to remove the outliers in order to improve the accuracy of the model. Equation 3 shows the final SR model developed from the beam fatigue test results.

$$SR = 2.0844 - 0.1386 * \log(E_o) - 0.4846 * \log(\varepsilon_t)$$
$$- 0.2012 * \log(N) + 1.4103 * \mathrm{Tanh}(0.8471 * RP)$$
$$+ 0.0320 * \log(E_o) * \log(\varepsilon_t) - 0.0954 * \log(E_o)$$
$$* \mathrm{Tanh}(0.7154 * RP) - 0.4746 * \log(\varepsilon_t)$$
$$* \mathrm{Tanh}(0.6574 * RP) + 0.0041 * \log(N) * \log(E_o)$$
$$+ 0.0557 * \log(N) * \log(\varepsilon_t) + 0.0689 * \log(N)$$
$$* \mathrm{Tanh}(0.259 * RP) \qquad (3)$$

where,

SR = stiffness ratio
E_o = initial flexural stiffness (ksi)
ε_t = applied tensile microstrain (the tensile portion of the tension-compression loading cycle, or half peak-to-peak) (10^{-6} in./in.)
RP = rest period (s)
N = number of loading cycles

The adjusted R^2 value of the model was 0.891. Figure 10 shows the predicted versus measured SR values of the model, which indicates an accurate prediction. The figure shows two clusters of data points, where the top cluster represents data 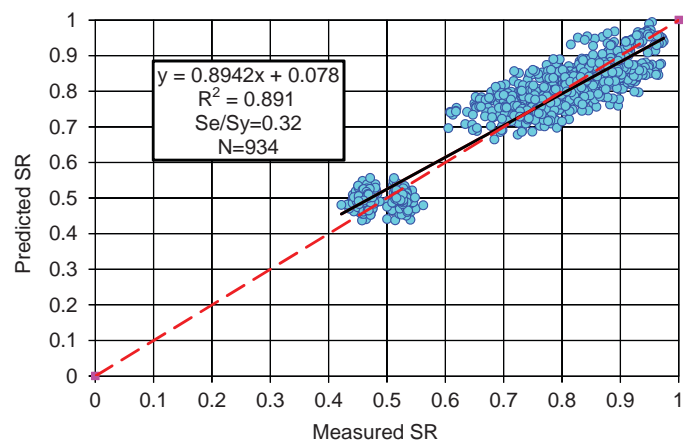with rest period and the bottom cluster represents data without rest period. A larger number of tests were performed with rest period since they produce results close to the endurance limit, which is the main outcome of the study. The two clusters of data represent a wide range of SRs producing a rational and stable regression model.

By substituting the SR in Equation 3 with 1.0 (complete healing condition), the strain becomes the endurance limit for different values of E_o, N, and RP.

Since N is included in the model, it is important to know how changing the value of N affects the endurance limit. A sensitivity analysis study was performed, where SR was plotted versus strain and rest period for different E_o values and three values of N (20,000, 100,000, 200,000 cycles). It was concluded that the number of loading cycles has little to no effect on the SR value, especially for rest periods higher than 1s and large values of N. This conclusion validates the assumption that complete healing occurs during the rest period after each load application, which makes the number of load applications redundant when the model is used to define the endurance limit strain. As a result, the endurance limit was calculated at a value of 200,000 cycles in the model. Note that aging is indirectly considered in Equation 3 since aging affects the stiffness of the mix.

Estimation of Endurance Limit Based on Beam Fatigue Testing Model

The endurance limit was estimated by plotting SR versus strain at rest periods of 1, 2, 5, 10, and 20s. In each case, the endurance limit was obtained as the strain corresponding to an SR value of 1.0, indicating complete healing during the rest period. Figure 11 provides examples of estimating the endurance limits at rest periods of 1 and 5s and SR = 1.0.

Figure 12 and Table 4 summarize the endurance limit values obtained from the model for several rest periods and stiffness values. The model produced endurance limit values of 22 microstrain to 223 microstrain for the variables analyzed
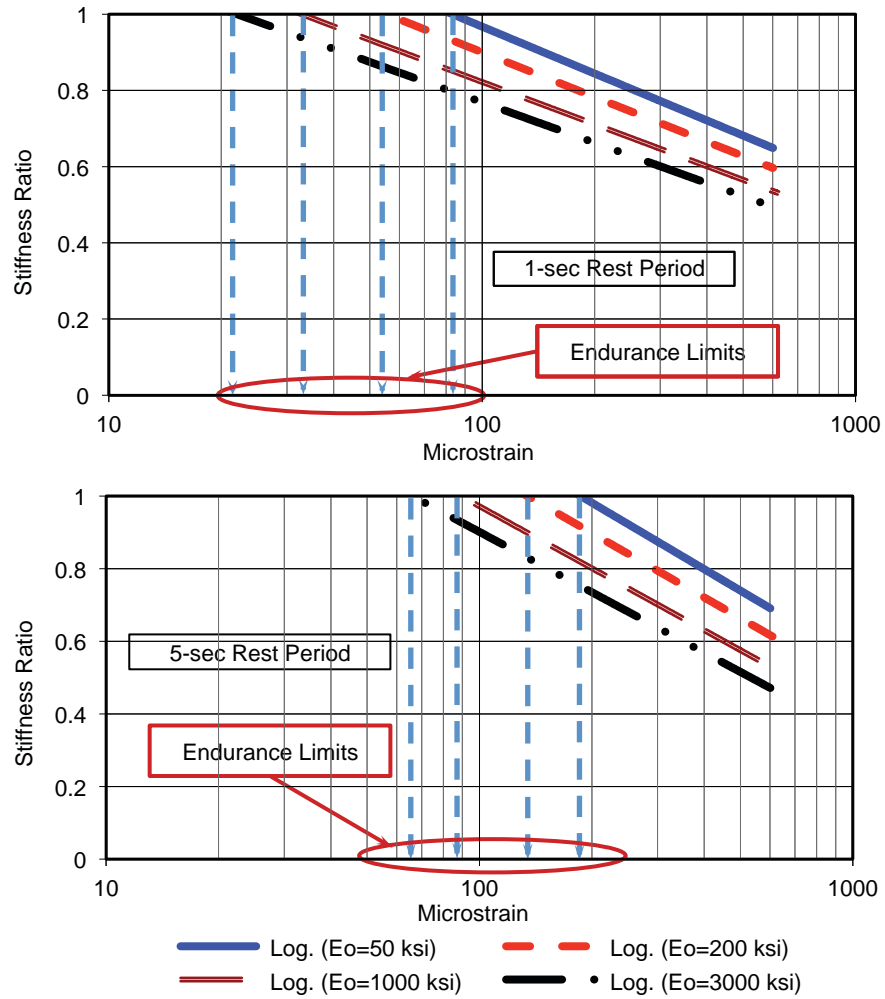
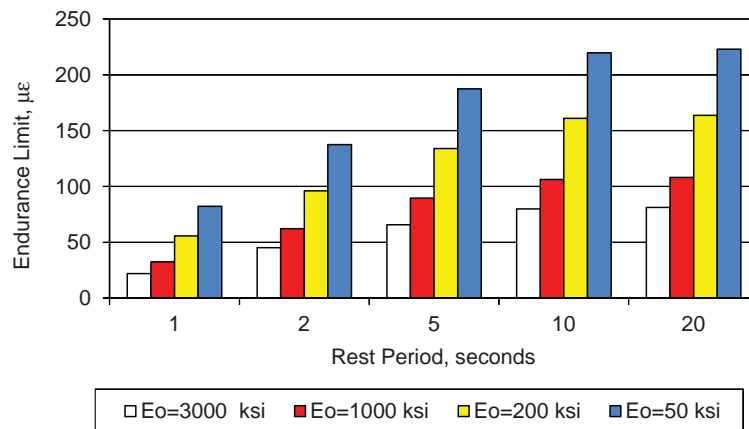*Figure 11. Examples of estimating the endurance limits for several initial stiffness values.*

Figure 12. Summary of endurance limit values versus several rest periods and stiffness values using the beam fatigue test model.

Table 4. Endurance Limits (EL) predicted from the beam fatigue test model.

Rest Period (seconds)	Stiffness (ksi)	Predicted EL (µε)	EL Range (µε)
1	3,000	22	22 – 82
	1,000	32	
	200	56	
	50	82	
2	3,000	45	45 – 138
	1,000	62	
	200	96	
	50	138	
5	3,000	66	66 – 187
	1,000	90	
	200	134	
	50	187	
10	3,000	80	80 – 220
	1,000	106	
	200	161	
	50	220	
20	3,000	81	81 – 223
	1,000	108	
	200	164	
	50	223	

(rest period and AC moduli [E_o]). The results show that decreasing the stiffness makes the material more ductile and, therefore, the endurance limit increases. Also, increasing the rest period increases the endurance limit. This means that the endurance limit at larger strains is obtained at longer rest periods in order to allow for complete healing. The endurance limit increased from a range of 22–82 microstrain at 1s rest period to a range of 81–223 microstrain at a 20s rest period. The endurance limit values at rest periods of 10 and 20s were almost the same. This suggests that the threshold rest period to complete the healing is between 5 and 10s for a loading period of 0.1s.

Figure 13 shows that the number of loading cycles has little or no effect on the SR value for tests with a rest period, especially at large values of N. Since the endurance limit is obtained at an SR value of 1.0, the number of loading cycles also has little or no effect on the endurance limit. As a result, the endurance limit was calculated at a value of 200,000 cycles in the rest of the study.
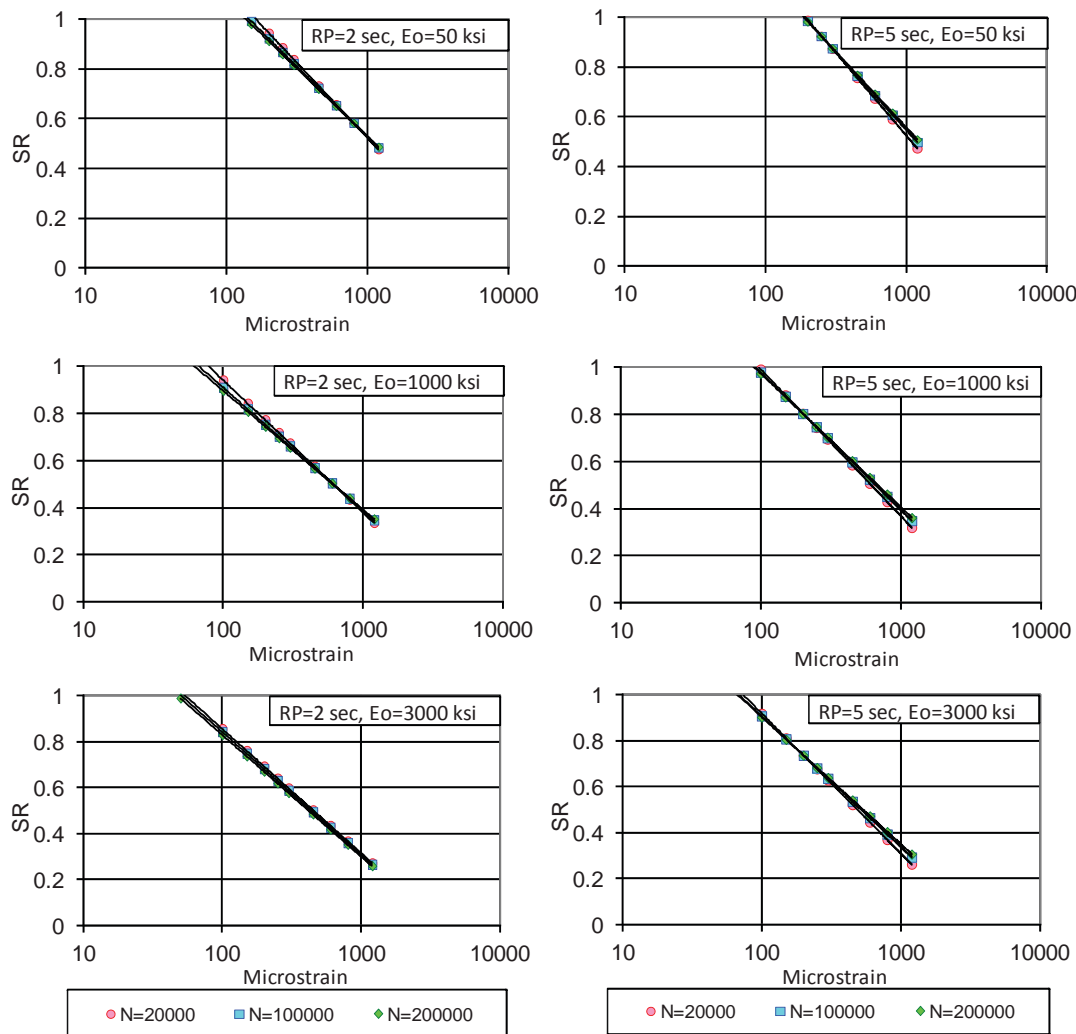

Figure 13. SR vs. strain at different values of rest period, stiffness, and number of load repetitions.

Developing of Endurance Limit Model Based on Uniaxial Fatigue Tests

The materials used in the uniaxial fatigue test were the same as those of the beam fatigue test, except that only one asphalt binder (PG 64-22) was used instead of three. The same factors and levels as in the beam fatigue experiment were used. The similarity of materials and factors between the uniaxial and the beam fatigue tests allows for direct comparisons of the results of the two test methods. Gyratory specimens were prepared with a 6-in. diameter and a 6.7-in. height using the Superpave gyratory compactor. Four-in. diameter specimens were cored from the gyratory compacted specimens and cut to a 6-in. height for complex modulus testing or cored to a 3-in. diameter and cut to a 6-in. height for the uniaxial test. Air voids were measured using the saturated surface-dry procedure (AASHTO T166, Method A). Any specimen with air voids deviating by greater than 1 percent from the target value of 7 percent was rejected.

Continuum Damage Approach

The Continuum Damage Mechanics (CDM) analysis approach was developed at North Carolina State University and Texas A&M University. This approach utilizes the viscoelastic correspondence principle and Work Potential Theory (WPT) described by Schapery (*29*) to remove viscous effects in monitoring changes in pseudo stiffness in repeated uniaxial tensile tests. Physical variables are replaced by pseudo variables based on the extended elastic-viscoelastic correspondence principle to transform a viscoelastic (linear or nonlinear) problem to an elastic case.

One of the viscoelastic properties required to apply the CDM approach is the relaxation modulus. The relaxation modulus is defined as the stress response of a viscoelastic material due to a unit step of strain input. The relaxation modulus can be calculated as the time-dependent stress divided by the initial applied strain as shown by Equation 4:

$$E(t) = \frac{\sigma(t)}{\varepsilon_o} \tag{4}$$

where $E(t)$ is the relaxation modulus at time t, $\sigma(t)$ is the stress at time t, and ε_o is the initial applied strain.

The calculation of the pseudo stiffness (PS) requires the calculation of pseudo strain (ε^R). The pseudo strain can be calculated rigorously using Equation 5, where ε is the measured strain, $E(t)$ is the linear viscoelastic relaxation modulus and E_R is the reference modulus (typically taken as 1) used for dimensional compatibility (*29*).

$$\varepsilon^R = \frac{1}{E_R} \int_0^t E(t-\tau) \frac{d\varepsilon}{d\tau} d\tau \tag{5}$$

Kim et al. (*30*) proposed a simplified approach for the steady-state assumption to calculate the pseudo strain as shown in Equation 6. This equation is based on the assumption that fatigue damage accumulates only under the tensile loading condition, represented by the pseudo strain tension amplitude, $\varepsilon_{0,ta}^R$. In such conditions, the pseudo strain can be rigorously computed as the product of strain and dynamic modulus, $|E^*|_{LVE}$ (at temperature and frequency matching with the test under investigation).

$$(\varepsilon_{0,ta}^R)_i = \frac{1}{E_R} \cdot \frac{\beta+1}{2} ((\varepsilon_{0,pp})_i \cdot |E^*|_{LVE}) \tag{6}$$

where β is a factor used to quantify the duration that a given stress cycle is tensile (1 means always tensile, 0 means fully reversed loading and −1 means always compressive), and $\varepsilon_{0,pp}$ stands for peak-to-peak strain amplitude.

Underwood et al. (*31*) suggested a simplified approach to calculate the pseudo strain. For the first loading path where damage growth may be significant, the rigorous calculation (*31*) is used; for the remaining cycles, the simplified calculation is used.

Once the pseudo strain is calculated, the PS is also calculated through Equation 7 using the pseudo strain as defined in Equations 5 and 6.

$$PS = \begin{cases} \dfrac{\sigma}{\varepsilon^{R} \times DMR} & \textit{first cycle} \\[3mm] \dfrac{\sigma}{\varepsilon^{R}_{0,ta} \times DMR} & \textit{rest of cycles} \end{cases} \quad (7)$$

where the DMR is the dynamic modulus ratio to account for specimen-to-specimen variability (*32*) and is defined as shown in Equation 8. In this equation $|E^*|_{LVE}$ is the linear viscoelastic dynamic modulus of the material at the particular temperature and frequency of the test and it can be determined from the $|E^*|$ master curve. $|E^*|_{fp}$ is the finger-print dynamic modulus that is measured from a fingerprint experiment performed before the uniaxial fatigue test.

$$DMR = \frac{|E^*|_{fp}}{|E^*|_{LVE}} \quad (8)$$

For the purpose of developing the Pseudo Stiffness Ratio (PSR) model using the continuum damage approach and predicting the endurance limit, two tests were performed: the complex modulus test and the uniaxial tension-compression fatigue test.

Complex Modulus Testing

The main objective of the complex modulus test was to construct the dynamic modulus master and phase angle master curves to estimate the relaxation moduli required in the analysis of the viscoelastic and continuum damage model. Four asphalt mixtures were tested in this part of the study representing combinations of two levels of asphalt content and two levels of air voids (4.2%AC-4.5%AV, 4.2%AC-9.5%AV, 5.2%AC-4.5%AV, and 5.2%AC-9.5%AV).
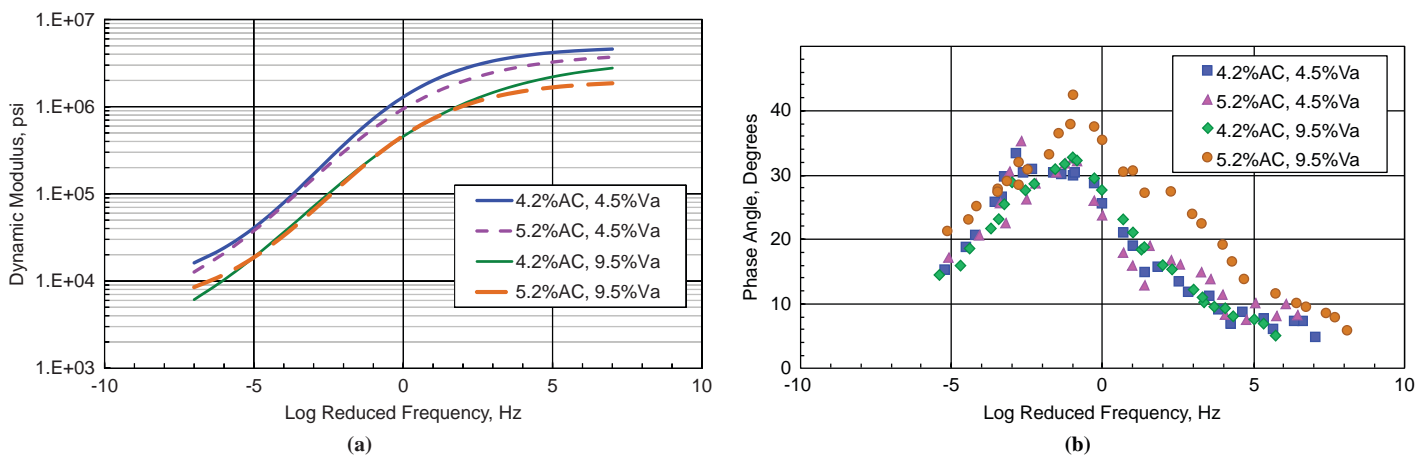
Complex modulus (E^*) tests were performed according to AASHTO TP 62-07 using a servohydraulic testing machine. Two replicates were tested for each factor combination. E^* tests were conducted on each specimen at a full sweep of loading frequencies (25, 10, 5, 1, 0.5 and 0.1 Hz) and temperatures (−10, 4.4, 21.1, 37.8 and 54.4°C). Using the E^* test results, i.e., the dynamic modulus, $|E^*|$, and the phase angle, ϕ, master curves were constructed for the four mixtures using the time-temperature superposition principles (Figure 14). It can be observed from Figure 14 that the $|E^*|$ values were more significantly affected by varying the air voids from 4.5 to 9.5% than by varying the asphalt content from 4.2 to 5.2%.

Uniaxial Fatigue Testing

In order to determine the strain values to be used in the uniaxial fatigue test, a pilot experiment was performed to establish the log N_f-log ε_t relationships for the four mixtures at three selected temperatures (40, 70, 100°F). These fatigue relationships were then used to determine the three tensile strain values used in the uniaxial fatigue experiments. The criterion for selecting the three tensile strain values at each temperature was to reach a fatigue life of 5,000, 20,000, and 100,000 cycles at the high, medium, and low tensile strain values, respectively. To establish a single fatigue relationship, four uniaxial tension-compression fatigue tests were conducted at different strain levels, which required 12 tests for one mixture at three temperatures (40, 70, and 100°F) or 48 tests for the four asphalt concrete mixtures. These fatigue relationships were then used to determine the tensile strain values for each mixture at the three temperatures.

Figure 14. (a) Dynamic modulus master curves and (b) phase angle master curves.

Waveform Selection

Similar to the beam fatigue test, the uniaxial fatigue test can be performed using a haversine (pull-pull) or a sinusoidal (pull-push) waveform. The rationale used in the beam fatigue test was also used in the uniaxial fatigue test, in which it was concluded that a haversine waveform cannot be maintained during the test on a viscoelastic material such as HMA. If a haversine tensile waveform is used, the gauge length of the specimen will change in such a way that the haversine waveform will change to sinusoidal after a few loading cycles. This would result in misleading results because of the inconsistency between the assumed condition (tension only with a peak-to-peak value) and the actual test conditions (tension and compression with a half peak-to-peak value). Therefore, a sinusoidal (pull-push or tension-compression) waveform was used in the uniaxial fatigue test.

Experimental Design

The uniaxial fatigue tests were conducted using the test protocol developed in Appendix 2 of this report. Figure 15(a) shows the system setup used to conduct the uniaxial fatigue test. The vertical deformation is measured with three spring-loaded on-specimen linear variable differential transformers (LVDTs) spaced 120 degrees apart. The LVDTs are attached to the specimen using parallel brass studs to secure the LVDTs in place. Three pairs of studs are glued on the surface of the specimen with gauge lengths of 4 in. Because of the difference between the actuator displacement and specimen displacement, on-specimen LVDTs had to be used considering the small displacement measurements used in this test.

After many trials and several gluing procedures, it was found that the uniaxial test is much more cumbersome and time consuming than the beam fatigue test. Several issues had to be addressed in order to perform successful tests. For example, the specimen has to be glued to the platens in order to subject the specimen to tension. The proper glue has to be selected in order to ensure that failure occurs in the specimen, and not at the interface between the specimen and the platen. Another important issue is specimen alignment. If there is any small eccentricity in the specimen, the specimen may break after a few loading cycles or may break too close to one of the platens and outside the gauge length. A special gluing jig was manufactured in order to carefully center the specimen when it is glued into the end platens as shown in Figure 15(b).

The uniaxial fatigue tests were conducted by controlling the on-specimen strain using a sinusoidal strain waveform (tension-compression). Similar to the beam fatigue experiment, some tests were performed without rest periods with a frequency of 10 Hz, while others used a 0.1s sinusoidal loading followed by a rest period. Fatigue failure was defined at 50% reduction of the initial stiffness.

As a part of the uniaxial test protocol, two special uniaxial fatigue software programs were developed by the IPC Company to conduct uniaxial fatigue tests without and with rest periods. The uniaxial fatigue test without rest period was conducted until fatigue failure occurred as discussed subsequently. However, all the tests with rest period were stopped at 20,000 cycles due to time limitations of the overall study.

In order to reduce the number of tests and at the same time determine important effects of all variables, a five-factor fractional factorial statistical design was used considering the effect of all five factors, two-factor interactions, and three-factor interactions (*27, 28*). Similar to the beam fatigue test, two or three replicates were tested for each factor combination. An analysis of the results from 132 tests was used to develop the model.

Model Development

Similar to the beam fatigue test, several initial regression models were tried. Originally, a regression model was developed to relate the PSR to all factors used in the study, which are binder content, air voids, temperature, applied tensile strain, rest period, and number of loading cycles. Later, the model was simplified by replacing the binder content, air voids, and temperature with the initial stiffness of the mixture.

The inclusion of the rest period decreases the stiffness deterioration through partial or full healing of fatigue damage. That is, the stiffness tends to deteriorate at a slower rate compared to the test without rest period. In this study, the PS values at different loading cycles were determined using the improved calculation methods developed by Underwood et al. (*31*). Because the PS varies between replicates, the PSR
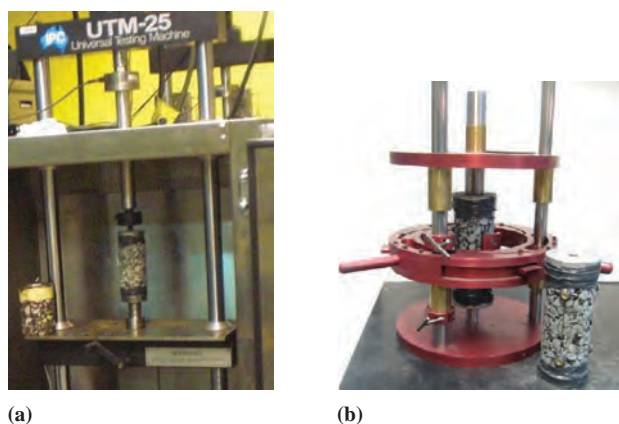

(a)   (b)

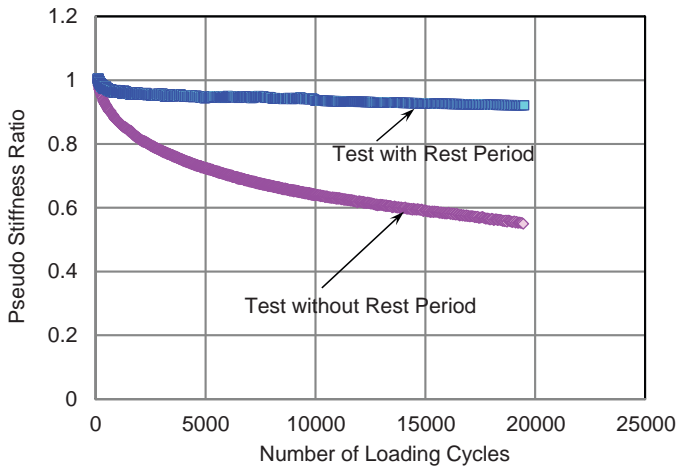***Figure 15. (a) Uniaxial fatigue test setup and (b) Gluing jig.***

Figure 16. Pseudo Stiffness Ratio (PSR) versus time relationship for tests with and without rest periods.

Figure 17. Effect of strain and rest period of the PSR as a function of the loading cycles.

was used, which is the PS value at any cycle (PS_n) normalized to the initial stiffness (PS_o). Figure 16 shows the relationship of PSR versus time for two tests conducted using 0 and 5s rest periods and a 310 peak-to-peak microstrain at 70°F.

In this part of the study, the PSR parameter was used to define the effect of rest period. For the test with rest period, decreasing the strain level or increasing the rest period would decrease the net fatigue damage and increase the PSR over time. If the test was conducted at specific tensile strain and rest period so that the fatigue damage created during loading is equal to the healing occurring during the rest period, the tensile strain is the endurance limit. This means that the PSR is equal to 1.0 at all loading cycles as demonstrated in Figure 17.

To determine the tensile strain value that represents the endurance limit when the net damage is zero (PSR = 1.0), the tensile strain versus the PSR at different temperatures and at a certain number of loading cycles is required. The endurance limit is calculated as the tensile strain value when this relationship intersects with PSR of 1.0 as shown in Figure 18.

The test results from all uniaxial fatigue experiments were combined together to develop the PSR model for the PG 64-22 mixture. For each test with rest period, four PSR values were measured at different N values on the PSR-N curve (Figure 16) to represent the nonlinear change of PSR over time. Only the PSR values at N_f were considered for the tests without rest period. A total number of 161 test results and 385 data points were used in the model development. The PSR model included the main five factors plus one additional factor, which is the value of N where the PSR was measured. A nonlinear optimization analysis was used considering one- and two-factor interactions in the statistical model. A powerful nonlinear optimization technique that uses innovative genetic algorithm (GA) technology was uti-
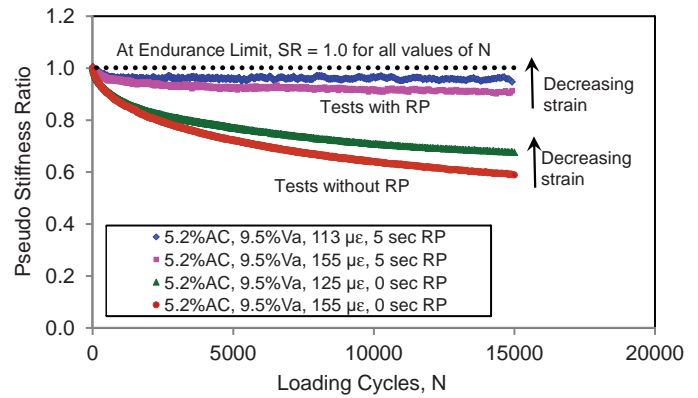
lized to provide an accurate optimization solution. Evolver®, a GA technology-based software that is well-suited to find the best overall answer by exploring the entire universe of possible answers, was used in this part of the study to develop the PSR model (*33*).

The optimization technique requires the main form of the regression model as an input. To construct a rational model, the relationship between the PSR and each factor was investigated by following an iteration process. It was found that there is a need for a logarithmic transformation for strain and number of loading cycles, while the second degree polynomial function was proper for temperature. For the rest period, a special function was used to fit its relationship with the PSR. The laboratory tests showed that increasing the rest period increases the PSR, indicating more healing. The rate of increase of PSR decreases as the rest period increases up to a certain threshold value above which there is no more PSR increase as shown in Figure 19. Using the tangent hyperbolic (Tanh) function to fit the PSR and rest period relationship, the threshold rest period can be found. The shape and form of the tangent hyperbolic
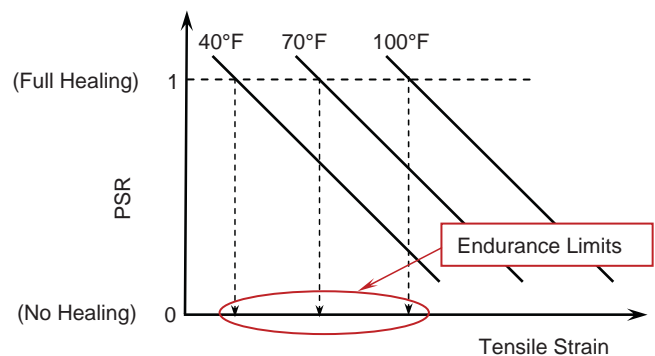

Figure 18. Determination of endurance limit at each temperature using PSR parameter.
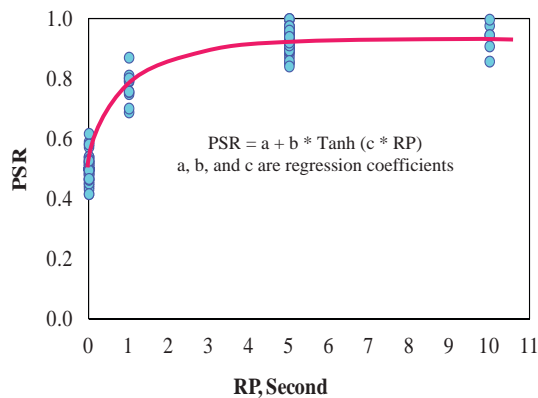
Figure 19. Effect of rest period on PSR.

Figure 20. Measured versus predicted PSR for the uniaxial fatigue test model.

function to fit the PSR and rest period relationship are presented in Figure 19.

In order to obtain a non-biased regression model, the sum of errors was set to zero. The model was further improved by removing the outlier data points using the method suggested by Montgomery (*28*). The analysis was then repeated based on the remaining 383 data points and the regression model shown in Equation 9 was obtained.

$$PSR = 0.459539 - 0.090917 * \log E_o - 0.104389 * \log \varepsilon_t$$
$$+ 0.417028 * Tanh\,(0.875884 * RP) + 0.238893 * \log N$$
$$+ 0.120018 * \log E_o * \log \varepsilon_t - 0.041502 * \log E_o * \log N$$
$$- 0.077377 * \log \varepsilon_t * \log N \qquad (9)$$

where,

   PSR = pseudo stiffness ratio
   E_o = initial flexural stiffness (ksi)
   ε_t = applied tensile microstrain (the tensile portion of the tension-compression loading cycle, or half peak-to-peak) (10^{-6} in./in.)
   RP = rest period (seconds)
   N = number of loading cycles

The adjusted R^2 value of the model was 0.951. Figure 20 presents the measured versus predicted PSR, which indicates accurate prediction. Similar to Figure 9, the two clusters of data points represent tests with and without rest periods.

For all the cases presented, it is clear that the PSR increases as the rest period increases up to a certain threshold value, after which the PSR is constant. The threshold rest period values for all the cases were around 3s for a loading time of 0.1s.

To investigate the effect of N on the PSR and consequently on the endurance limit, the PSR versus the tensile strain relationships were investigated at different RP, N values of 25,000, 50,000, 100,000, and 200,000 loading cycles, and
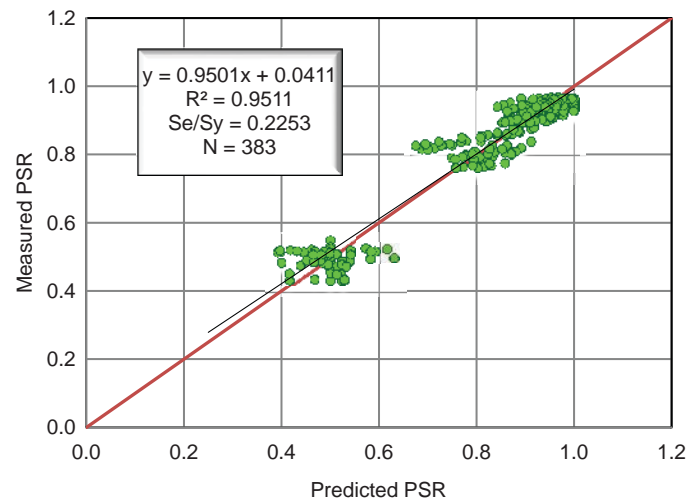
temperatures of 40, 70, and 100°F for the four asphalt mixtures. Unlike the results of the beam fatigue study, the results showed that PSR-tensile strain relationships are not parallel at different N values.

Estimation of Endurance Limit Based on Uniaxial Fatigue Testing Model

The PSR model was used to predict the PSR values (when PSR is 1.0) at different tensile strain values for each mixture type at different temperatures. The endurance limit was estimated by plotting PSR versus strain at rest periods of 1, 2, 5, 10, and 20s. In each case, the endurance limit was obtained as the strain corresponding to a PSR value of 1.0, indicating complete healing during the rest period. Figure 21 demonstrates examples of stiffness ratio versus strain for rest periods of 1 and 5s.

Figure 22 and Table 5 demonstrate the endurance limit values for different stiffness and rest period values at N = 20,000 cycles. It can be observed that the mixtures with higher stiffness showed lower endurance limit as expected. In addition, the endurance limit values were stable after 5s of rest period. The threshold rest period occurred at about 3s. The number of loading cycles, N, has a slight effect on the endurance limit values, where higher N showed slightly higher endurance limit values.

Figure 23 shows the relation between the PSR and the tensile strain at different numbers of loading cycle. The figure shows that the number of loading cycles has little effect on the PSR value. The endurance limit was calculated at 20,000 cycles for the uniaxial model.
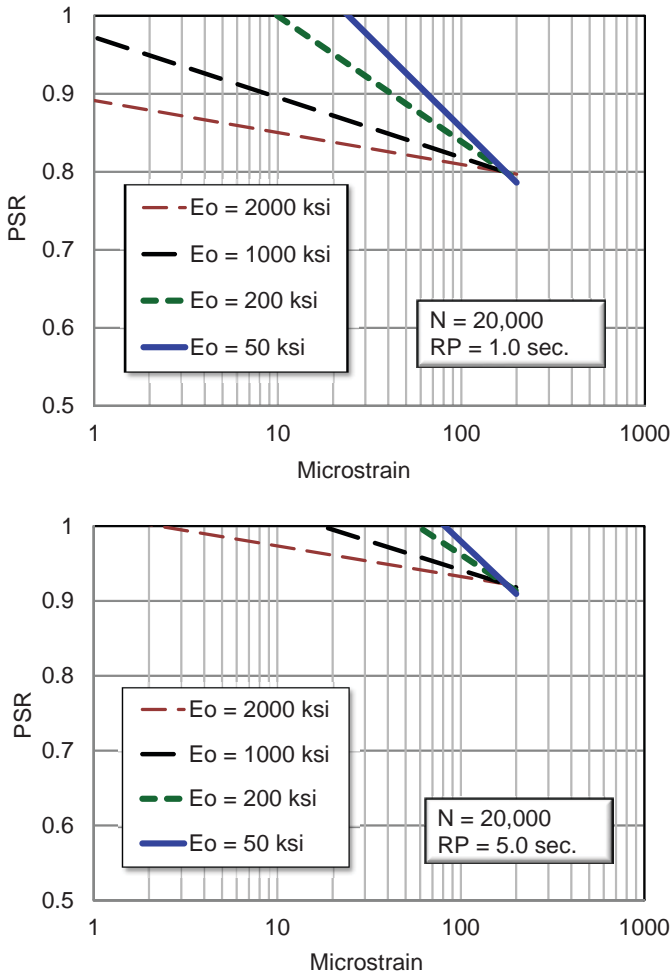
Table 5. Endurance Limits (EL) predicted from the uniaxial fatigue test model.

Rest Period (seconds)	Stiffness (ksi)	Predicted EL (με)	EL Range (με)
1	2,000	1	1-25
	1,000	1	
	200	10	
	50	25	
2	2,000	1	1-65
	1,000	9	
	200	42	
	50	65	
5	2,000	3	3-82
	1,000	18	
	200	59	
	50	82	
10	2,000	3	3-82
	1,000	18	
	200	59	
	50	82	
20	2,000	3	3-82
	1,000	18	
	200	59	
	50	82	

Figure 21. PSR versus tensile strain at different initial stiffness values for 1-second and 5-second rest periods.

Figure 22. Endurance limit values at different rest periods and stiffness values using uniaxial fatigue test model (N = 20,000).

Figure 23. Effect of N on PSR at different initial stiffness and RP values.

CHAPTER 4

Recommended Fatigue Test and Endurance Limit Implementation

Comparison of Endurance Limits of Beam and Uniaxial Fatigue Tests

The beam fatigue model was developed using three binders (PG 58-28, PG 64-22, PG 76-16), while the uniaxial test model was developed using one binder only (PG 64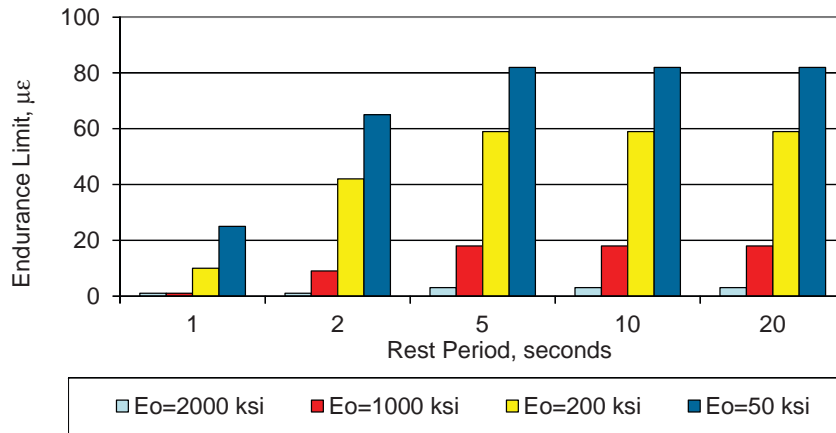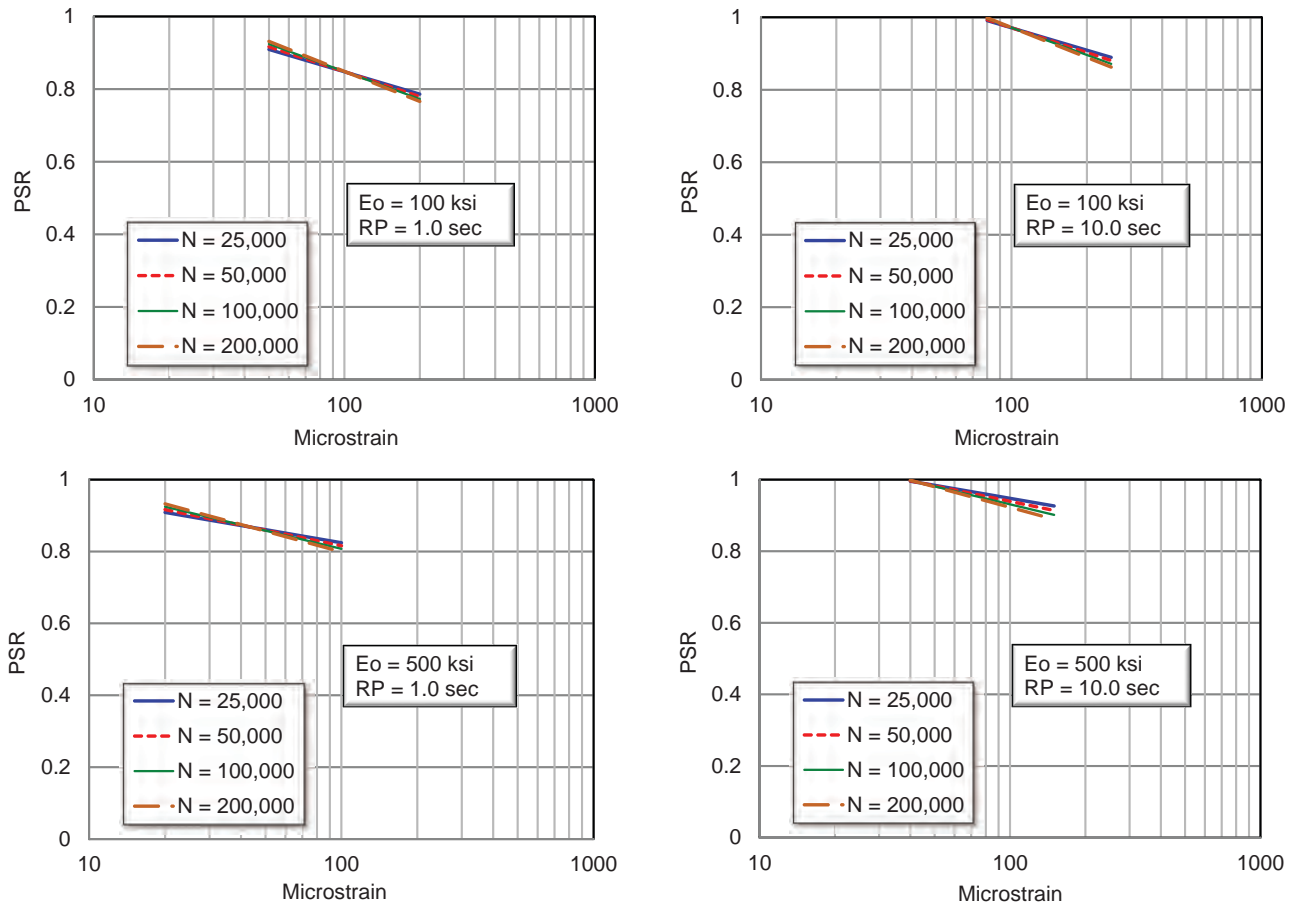-22). Since the beam and uniaxial fatigue tests produce different types of stresses, they produce different endurance limit values as shown in Tables 4 and 5.

In order to have a fair comparison between the endurance limits of beam and uniaxial fatigue tests, only the beam fatigue data of the PG 64-22 mixture were used to develop a new beam fatigue model to predict the SR in the form of Equation 2. The model was then used to estimate the endurance limit values at different temperatures when the SR-ε_t relationships reach an SR value of 1.0. The results of the beam fatigue model were compared with the results of the uniaxial fatigue model in the same form (Equation 2). The results showed that the endurance limit values of the two tests exhibit similar trends. The endurance limits obtained from the uniaxial fatigue model are about 10% less than those obtained from the beam fatigue model when the same binder was used. This comparison showed that, regardless of the fatigue test type, the asphalt mixtures are prone to heal in a similar fashion if allowed to rest.

Figure 24 includes a direct comparison of the endurance limit values obtained from the beam fatigue model and the uniaxial fatigue model using the same binder. These values were estimated for all mixtures at a 5s rest period, 20,000 loading cycles, and three temperatures (40, 70, and 100°F). It is clear that there is a good correlation between the endurance limit values from both models when the same binder is used.

It must be recognized that simplifying the models by replacing the binder grade, binder content, air voids, and temperature with the stiffness of the material may produce a certain level of inaccuracy. For example, mixtures with high binder content and low air voids showed similar stiffness to those that have low binder content and high air voids, even though their endurance limits are different. This stiffness effect became more apparent in the uniaxial PSR model since it covered a narrow range of stiffness (one binder grade only), while the beam fatigue model covered a wide range of stiffness (three binder grades), which reduced the impact of the stiffness effect. This observation may explain the difference between the endurance limits obtained from the two stiffness-based models as shown in Figures 12 and 22 (Tables 4 and 5).

As indicated earlier, the uniaxial test is more time consuming than the beam fatigue test and requires an enormous attention to details. Uniaxial specimens have to be carefully glued to the loading platens and properly aligned in the loading machine in order to avoid improper or premature failure. In addition, the beam fatigue test is more established with a larger database available in the literature than the uniaxial test. Finally, it is most important to understand that all pavement fatigue cracking subsystems in mechanistic design procedures for asphalt concrete are based upon tensile strain generated in the pavement by a repetitive flexing of the layer. As a consequence, it is suggested that the future endurance limit studies utilize beam fatigue tests.

Incorporating the Endurance Limit in Fatigue Relationships

The fatigue relationships shown in the literature are typically parallel straight lines for different E_o values on a log-log graph as shown in Figure 25. These lines show that when the applied strain decreases, the number of load applications to failure (N_f) increases following a log-log relationship, without consideration of an endurance limit. The endurance limit obtained from the beam fatigue model developed in this study (Equation 3) can be easily and directly incorporated in the fatigue relationships for a specific rest period as demonstrated in Figure 25. This means that if the applied strain is above the endurance limit, damage will accumulate and the asphalt layer will last up to a certain value of N_f. However, if
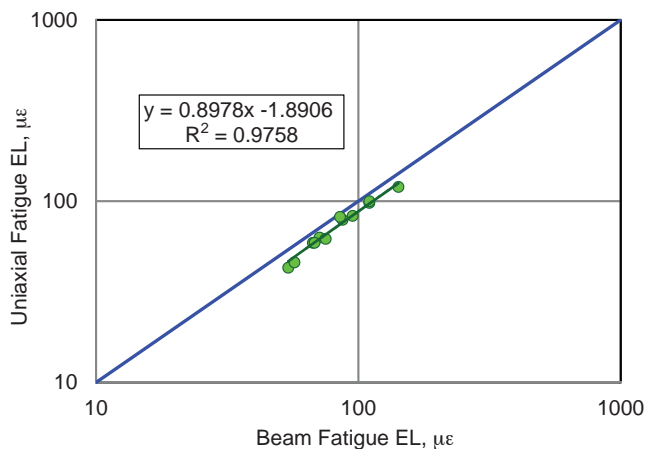
Figure 24. Comparison of endurance limit values obtained from uniaxial fatigue and beam fatigue models (PG 64-22, RP = 5s, N = 20,000 cycles).

the strain is below the endurance limit value and is applied at a certain rate (for a specific rest period), complete healing will occur and damage will not accumulate. This concept has a significant implication on extending pavement life, where the layer thicknesses and material properties can be controlled so that the strain does not exceed the endurance limit for the
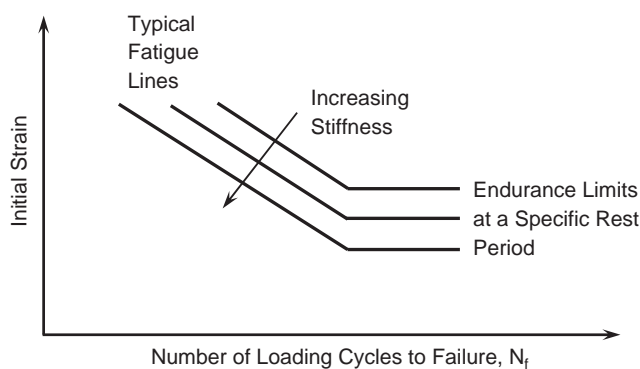

Figure 25. Incorporating endurance limits in fatigue relationships.

expected load spacing (rest period) of the design truck density in the total traffic stream.

Figure 25 also shows that when the material stiffness increases, N_f decreases if the strain is above the endurance limit. It also shows that when the material stiffness increases, the endurance limit decreases. The figure demonstrates the endurance limit concept for a specific rest period that corresponds to a specific AADTT in the field. If the rest period increases, complete healing will occur at larger strains and the endurance limit values will increase.

Incorporating the Endurance Limit in the Pavement ME Design

The current AASHTOWare Pavement ME Design does provide the effect of an endurance limit to be incorporated into the analysis. The designer is required to input a single value of endurance limit. As shown earlier, the endurance limit values vary depending on the material stiffness and the rest period between loading cycles. The incorporation of the beam fatigue endurance limit, developed from this project, into the ME Design will require additional software code to calculate the endurance limit value for the rest period associated with the typical design truck traffic spectra on the facility within the models developed in this project. However, this task of revising the software should be a relatively simple endeavor to accomplish.

At the same time, the critical strain value of the HMA layer (or sublayer) can be calculated using the Jacob Uzan Layered Elastic Analysis (JULEA) multilayer elastic computer program already incorporated in the ME Design software. If the critical strain calculated from the JULEA program is less than the fatigue endurance limit, the average axle is not counted in the analysis for this period, which means that there is no fatigue damage during this time period. However, if the critical strain is greater than the fatigue endurance limit, the average axle is counted as causing cumulative fatigue damage during this period.

CHAPTER 5

Summary and Findings

The concept of a perpetual pavement requires the knowledge of the HMA endurance limit. The main purpose of this study was to validate the endurance limit for HMA using laboratory beam and uniaxial fatigue tests with rest periods between loading cycles and develop the mathematical algorithm to insert this endurance limit into a predictive fatigue damage methodology. A comprehensive study was performed to estimate the endurance limit of a wide range of conventional HMA due to healing that occurs during the rest periods. Extensive laboratory displacement-controlled beam and uniaxial tension-compression fatigue tests were performed. Hot mix asphalt was used with three binder grades, two binder contents, two levels of air voids, three test temperatures, four values of rest periods between loading cycles, and three levels of applied strain. A fractional factorial statistical design was used in order to minimize the number of tests and still obtain the necessary results.

The study used the principle that the endurance limit occurs due to healing of the asphalt mix that happens during the rest period between loading cycles or stress pulses due to moving traffic. Two models were developed from the beam and uniaxial fatigue tests that can predict the SR or the PSR at various test conditions which can be related to the healing gained during the rest period. The strain that allows for complete healing was obtained to estimate the endurance limit below which a very large number of load repetitions (technically an infinite number) can be applied to the pavement without accumulation of fatigue damage. After developing the models, a concept of integrating the endurance limit in the traditional strain-N_f fatigue relationships was discussed as a step toward incorporating the endurance limit in the AASHTOWare Pavement ME Design.

The following are the key findings of this study.

1. HMA exhibits an endurance limit that varies with mixture properties, temperature, and pavement design conditions. There is no single value of the endurance limit for all conditions. The endurance limit varies depending on binder grade, binder content, air voids, temperature, and the rest period between load applications.

2. Mixtures using softer binders exhibit higher endurance limits than mixtures using stiffer binders.

3. High binder contents and low air voids produced high endurance limit values compared to low binder contents and high air voids, which showed low endurance limits.

4. Endurance limit values were higher at high temperatures, which correspond to soft mixtures compared to low temperatures that correspond to stiff mixtures.

5. HMA stiffness (modulus) was found to be an excellent surrogate property that takes into account all of the primary mix variables: binder grade, binder content, air voids, and temperature. This concept, however, needs to be used carefully since air voids and binder content can counteract each other and create the same stiffness but may have different endurance limits. However, it should also be recalled that the classical AC fatigue model used in the AASHTO ME Design also additionally adjusts fatigue life through the mix air void and effective bitumen contents.

6. For a loading period of 0.1s the rest period that ensures complete healing ranges from 5 to 10s for the beam fatigue results. The uniaxial fatigue results showed a threshold value of 3s.

7. The models developed in this project can accurately estimate the endurance limit without testing beyond 20,000 cycles if the rest period is adequately long (3 to 10s). The number of loading cycles has little effect on the endurance limit for tests with long rest periods since damage will be healed by the end of each loading cycle.

8. The endurance limit values from the beam fatigue test yielded differing strain magnitudes compared to those of the uniaxial fatigue test. The predicted endurance limit values based on the beam fatigue model with three binders ranged from 22 microstrain to 223 microstrain. The

endurance limit values based on the uniaxial fatigue model with one binder ranged from 1 microstrain to 82 microstrain. It would be desirable to determine if expanding the uniaxial endurance limit study to the same three binders would result in a more favorable comparison of the endurance limit values of the two tests.

9. The beam fatigue model (Equation 3) is proposed for future endurance limit studies. The beam fatigue test is more established with a larger database available in the literature than the uniaxial test. The model obtained from the uniaxial test study (Equation 9) was based on limited data. Moreover, the uniaxial test is more time consuming than the beam fatigue test and requires an enormous attention to detail.

10. The endurance limit model obtained in this study from the flexural beam fatigue approach can be incorporated in Pavement ME Design. This would support the future design of perpetual pavements that could accommodate a large number of truck loads without accumulated fatigue damage. Such designs would require close control of layer thicknesses and material properties so that the strain does not exceed the endurance limit for the expected load spacing (rest period).

Suggested Future Research

This research developed an integrated model to predict healing and endurance limits for conventional HMA mixtures. To gain a better understanding of the endurance limit for the full range of asphalt mixtures, suggested future research includes:

- Field verification of the model for a wide variety of pavement cross sections and different combinations of HMA stiffness, rest period, and number of load applications. Verification can best be achieved by using existing databases, such as the LTPP, or using accelerated loading facilities to control critical design properties.
- Coding of the model for its incorporation in the AASHTO-Ware Pavement ME Design software.
- Investigation of the healing-based endurance limit method for other types of mixes such as recycled asphalt pavement, recycled asphalt shingles, warm mix asphalt, asphalt rubber, and mixtures prepared with polymer modified or highly chemically modified asphalt binders.
- Investigation of the contribution of the different components of the mix such as binder, mastic, and aggregate to the endurance limit.

References

1. Monismith, C. L., and D. B. McLean. "Structural Design Considerations," Proceedings of the Association of Asphalt Paving Technologists, Vol. 41, 1972.

2. Nishizawa, T., S. Shimeno, and M. Sekiguchi. "Fatigue Analysis of Asphalt Pavements with Thick Asphalt Mixture Layer," Proceedings of the 8th International Conference on Asphalt Pavements, Vol. 2. University of Washington, Seattle, WA, August 1997, pp. 969–976.

3. Wu, Z., Z. Q. Siddique, and A. J. Gisi. "Kansas Turnpike—An Example of Long Lasting Asphalt Pavement," Proceedings, International Symposium on Design and Construction of Long Lasting Asphalt Pavements. National Center for Asphalt Technology, Auburn, AL, 2004, pp. 857–876.

4. Bhattacharjee, S., A. Swamy, and J. Daniel. Application of Elastic–Viscoelastic Correspondence Principle to Determine Fatigue Endurance Limit of Hot-Mix Asphalt. In *Transportation Research Record: Journal of the Transportation Research Board, No. 2126,* Transportation Research Board of the National Academies, Washington, D.C., 2009, pp. 12–18.

5. Carpenter, S., H. K. Ghuzlan, and S. Shen. Fatigue Endurance Limit for Highway and Airport Pavements. In *Transportation Research Record: Journal of the Transportation Research Board, No. 1832,* Transportation Research Board of the National Academies, Washington, D.C., 2003, pp. 131–138.

6. Thompson, M. R., and S. H. Carpenter. "Considering Hot-Mix-Asphalt Fatigue Endurance Limit in Full-Depth Mechanistic-Empirical Pavement Design," International Conference on Perpetual Pavement, Columbus, OH, 2006.

7. Prowell, B. et al. "Endurance Limit of Hot Mix Asphalt Mixtures to Prevent Fatigue Cracking in Flexible Pavements," NCHRP Project 9-38, Updated Draft Final Report, NCHRP, Washington, DC, May 2008.

8. Advanced Asphalt Technologies, LLC. "Hot Mix Asphalt Endurance Limit Workshop: Executive Summary," National Cooperative Highway Research Program Project 9-44, November, 2007.

9. Carpenter, S. H., and S. Shen. A Dissipated Energy Approach to Study HMA Healing in Fatigue. In *Transportation Research Record: Journal of the Transportation Research Board, No. 1970,* Transportation Research Board of the National Academies, Washington, D.C., 2006, pp. 178–185.

10. Kim, B., and R. Roque. Evaluation of Healing Property of Asphalt Mixtures. In *Transportation Research Record: Journal of the Transportation Research Board, No. 1970,* Transportation Research Board of the National Academies, Washington, D.C., 2006, pp. 84–91.

11. Phillips, M. C. "Multi-Step Models for Fatigue and Healing, and Binder Properties Involved in Healing." Proceedings, Eurobitume Workshop on Performance Related Properties for Bituminous Binders, Luxembourg, Paper No. 115, 1998.

12. Kim, Y. R., and D. N. Little. Evaluation of Healing in Asphalt Concrete by Means of the Theory of Nonlinear Viscoelasticity. In *Transportation Research Record 1228,* TRB, National Research Council, Washington, DC, 1989, pp. 198–210.

13. Advanced Pavement Laboratory. NCHRP Project 9-44 Research Plan, Washington, DC, Nov. 2008.

14. SHRP, A-404. *Fatigue Response of Asphalt-Aggregate Mixes.* Strategic Highway Research Program, National Research Council, Washington, DC, 1994.

15. Harvey, J., and B.-W. Tsai. Effects of Asphalt Content and Air Void Content on Mix Fatigue and Stiffness. In *Transportation Research Record 1543,* TRB, National Research Council, Washington, DC, 1996, pp. 38–45.

16. Tayebali, A. A., G. M. Rowe, and J. B. Sousa. "Fatigue Response of Asphalt Aggregate Mixtures." *Journal of the Association of Asphalt Paving Technologists,* Vol. 61, 1994, pp. 333–360.

17. Verstraeten, J., J. E. Romain, and V. Veverka. "The Belgian Road Research Center's Overall Approach Structural Design." Fourth International Conference on the Structural Design of Asphalt Pavements, Vol. 1, Proc., Ann Arbor, MI, Aug 1977.

18. Van Dijk, W., and W. Visser. "The Energy Approach to Fatigue for Pavement Design." Proceedings Journal of the Association of Asphalt Paving Technologists Vol. 46, 1977, pp. 1-40.

19. Monismith, C. L., K. E. Secor, and W. Blackmer. "Asphalt Mixture Behavior in Repeated Flexure." Proceedings of Association of Asphalt Paving Technologists, Vol. 30, 1961, pp. 188–222.

20. Raithby, K. D., and A. B. Sterling. "Some Effects of Loading History on the Performance of Rolled Asphalt." TRRL-LR 496, Crowthorne, England, 1972.

21. Bonnaure, F., A. H. J. J. Huibbers, and A. Booders. "A Laboratory Investigation of the Influence of Rest Periods on Fatigue Characteristics of Bituminous Mixes." Proceedings, the Association of Asphalt Paving Technologists, Vol. 51, 104, 1982.

22. Uniform Standard Specifications for Public Works Construction Sponsored and Distributed by the Maricopa Association of Governments, Phoenix, AZ, 2011.

23. Witczak, M. W., M. S. Mamlouk, and M. A. Abojaradeh. *Superpave Support and Performance Models Management.* NCHRP Project 9-19, Task F – Evaluation Tests, Flexure Fatigue Tests. Department of Civil and Environmental Engineering, Arizona State University, Tempe, AZ, July 2001.

24. Mamlouk, M., M. Souliman, W. Zeiada, and K. Kaloush. "Refining Conditions of Fatigue Testing of Hot Mix Asphalt." *ASTM Journal of Advances in Civil Engineering Materials,* Vol. 1, Issue 1, http://www.astm.org/DIGITAL_LIBRARY/JOURNALS/ACEM/PAGES/ACEM20120018.htm, Nov. 2012.

25. Pronk, A. C. "Comparison of 2 and 4 Point Fatigue Tests and Healing in 4 Point Dynamic Bending Test Based on the Dissipated Energy Concept." 8th International Conference on Asphalt Pavements, Seattle, WA, 1997.

26. Pronk, A. C. "Haversine Fatigue Testing in Controlled Deflection Mode: Is It Possible?" Presented at the Transportation Research Board 89th Annual Meeting, 2010.

27. JMP® software, SAS Institute Inc., http://www.jmp.com/.

28. Montgomery, D. C. *Design and Analysis of Experiments, 8th Edition.* John Wiley & Sons, Inc., Hoboken, NJ, 2013.

29. Schapery, R. A. Correspondence Principles and a Generalized J Integral for Large Deformation and Fracture Analysis of Viscoelastic Media. *International Journal of Fracture,* Vol. 25, 1984, pp. 195–223.

30. Kim, Y. R., D. N. Little, and R. L. Lytton. Fatigue and Healing Characterization of Asphalt Mixtures. *Journal of Materials in Civil Engineering,* ASCE, Vol. 15, No. 1, 2003, pp. 75-83.

31. Underwood, B. S., Y. R. Kim, and M. N. Guddati. Improved Calculation Method of Damage Parameter in Viscoelastic Continuum Damage Model. *International Journal of Pavement Engineering,* Vol. 11, Issue 6, December 2010, pp. 459–476.

32. Daniel, J. S., and Y. R. Kim. Development of a Simplified Fatigue Test and Analysis Procedure Using a Viscoelastic, Continuum Damage Model. *Journal of the Association of Asphalt Paving Technologists,* Vol. 71, 2002, pp. 619–650.

33. Evolver Software, http://www.palisade.com/evolver/.

A P P E N D I X E S 1 , 2 , A N D 3

Unpublished Material

Appendixes 1 through 3 as submitted by the research agency are not provided herein but are available on the TRB website (http://trb.org) and can be found by searching for *NCHRP Report 762.* The appendix titles are as follows:

Appendix 1:   Integrated Predictive Model for Healing and Fatigue Endurance Limit for Asphalt Concrete

Appendix 2:   Endurance Limit for HMA Based on Healing Phenomena Using Viscoelastic Continuum Damage Analysis

Appendix 3:   Project Lab Test Results Inserted into the Mechanistic Empirical Distress Prediction Models (M-E_DPM) Database

Abbreviations and acronyms used without definitions in TRB publications:

A4A	Airlines for America
AAAE	American Association of Airport Executives
AASHO	American Association of State Highway Officials
AASHTO	American Association of State Highway and Transportation Officials
ACI–NA	Airports Council International–North America
ACRP	Airport Cooperative Research Program
ADA	Americans with Disabilities Act
APTA	American Public Transportation Association
ASCE	American Society of Civil Engineers
ASME	American Society of Mechanical Engineers
ASTM	American Society for Testing and Materials
ATA	American Trucking Associations
CTAA	Community Transportation Association of America
CTBSSP	Commercial Truck and Bus Safety Synthesis Program
DHS	Department of Homeland Security
DOE	Department of Energy
EPA	Environmental Protection Agency
FAA	Federal Aviation Administration
FHWA	Federal Highway Administration
FMCSA	Federal Motor Carrier Safety Administration
FRA	Federal Railroad Administration
FTA	Federal Transit Administration
HMCRP	Hazardous Materials Cooperative Research Program
IEEE	Institute of Electrical and Electronics Engineers
ISTEA	Intermodal Surface Transportation Efficiency Act of 1991
ITE	Institute of Transportation Engineers
MAP-21	Moving Ahead for Progress in the 21st Century Act (2012)
NASA	National Aeronautics and Space Administration
NASAO	National Association of State Aviation Officials
NCFRP	National Cooperative Freight Research Program
NCHRP	National Cooperative Highway Research Program
NHTSA	National Highway Traffic Safety Administration
NTSB	National Transportation Safety Board
PHMSA	Pipeline and Hazardous Materials Safety Administration
RITA	Research and Innovative Technology Administration
SAE	Society of Automotive Engineers
SAFETEA-LU	Safe, Accountable, Flexible, Efficient Transportation Equity Act: A Legacy for Users (2005)
TCRP	Transit Cooperative Research Program
TEA-21	Transportation Equity Act for the 21st Century (1998)
TRB	Transportation Research Board
TSA	Transportation Security Administration
U.S.DOT	United States Department of Transportation